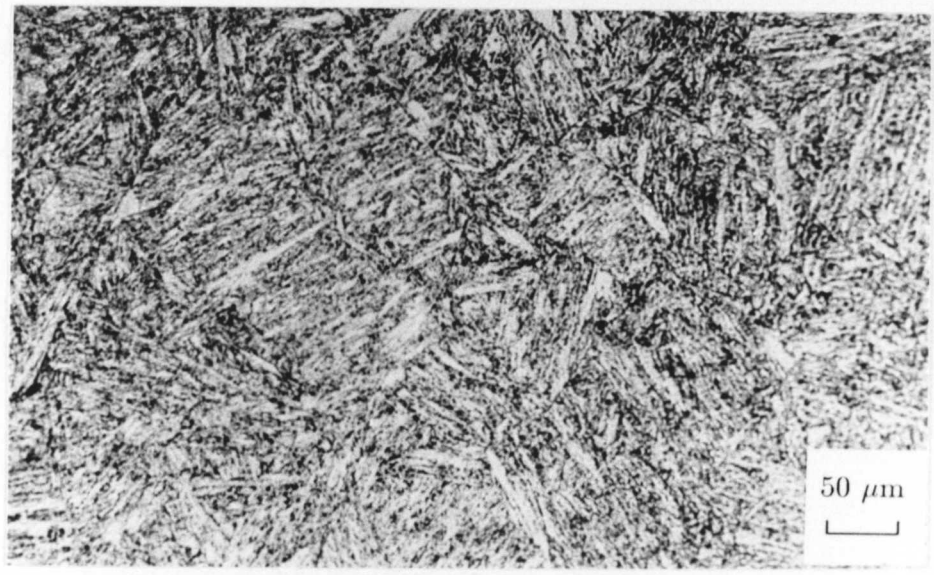

Figure 7.1: Optical micrograph for specimen austenitised at 1060°C 15 mins, air cooled, and tempered for 2 hours at 700°C.

a)

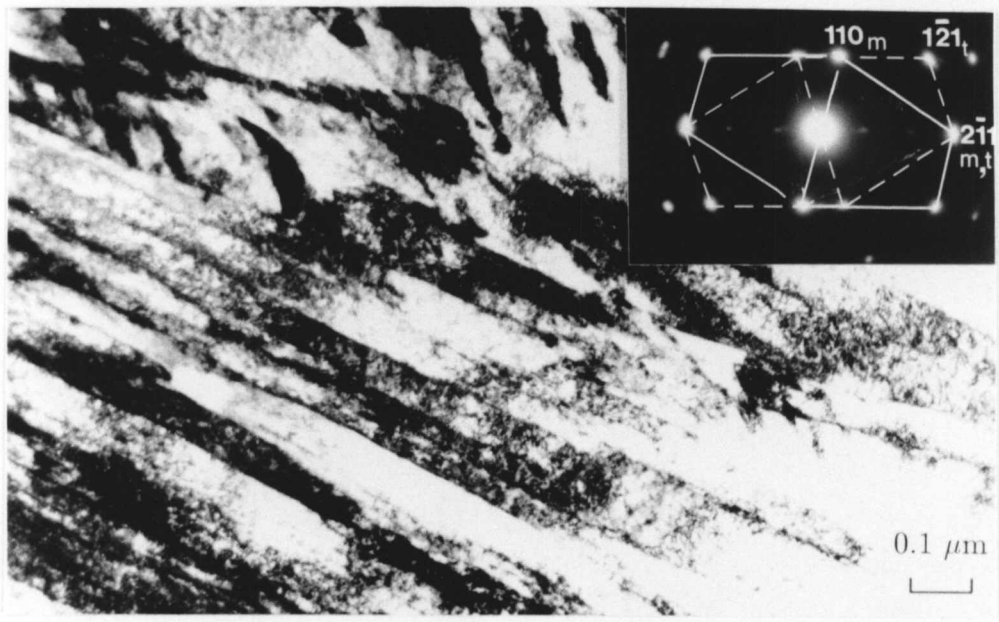

b)

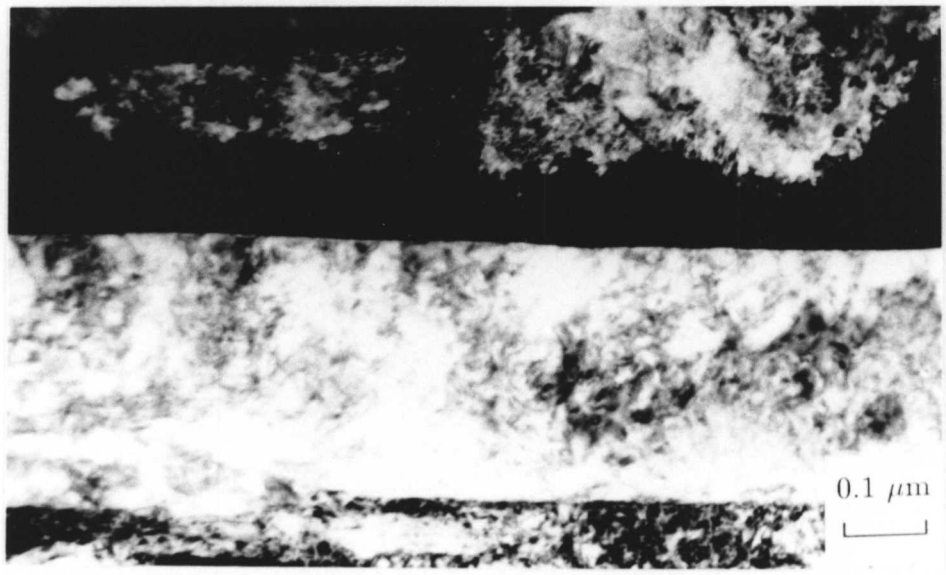

Figure 7.2: Transmission electron micrographs from the as–quenched microstructure. a) illustrates the twinned martensite microstructure; the inset is a selected area diffraction pattern showing the twin (t) and matrix (m) reflections. The twin plane is $2\bar{1}1$. b) is a higher magnification image showing that no auto–tempering has occurred.

a)

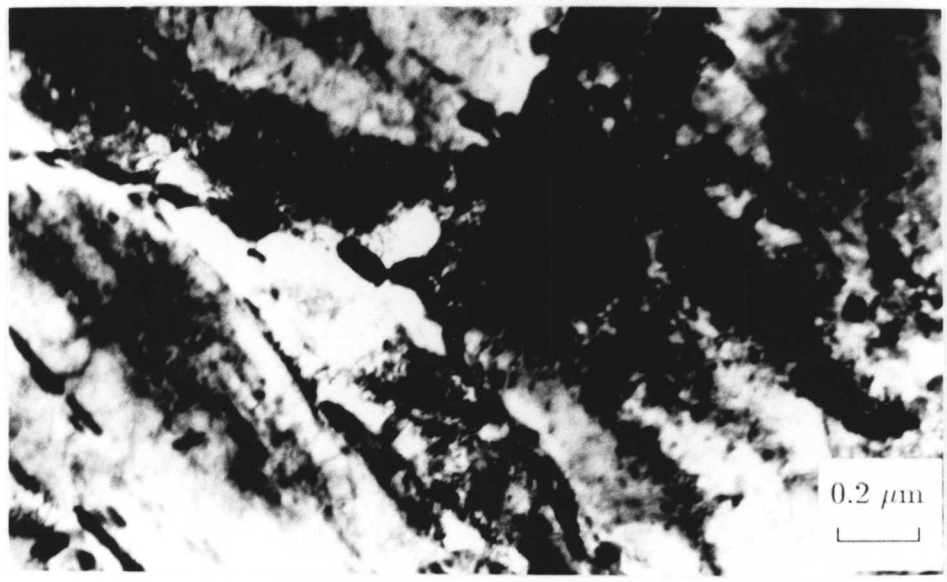

b)

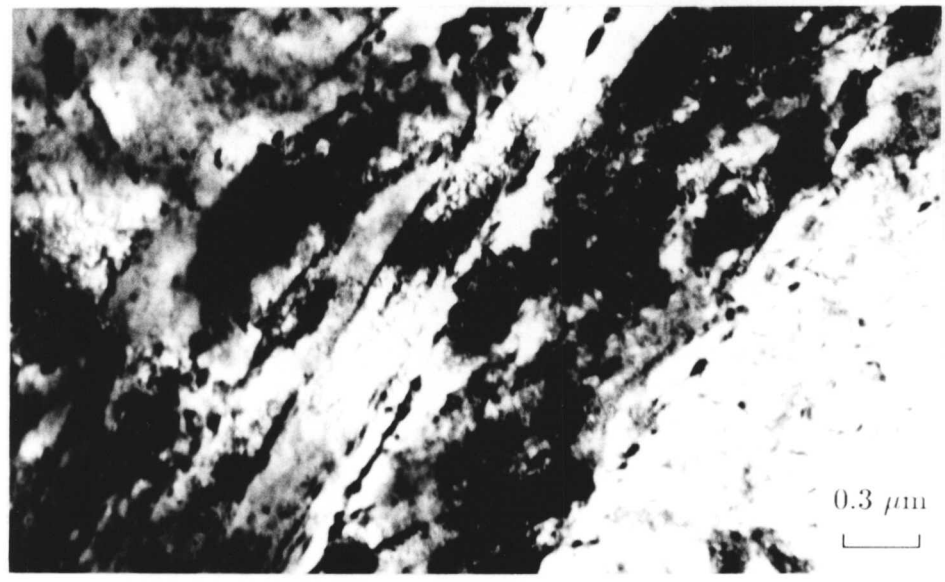

Figure 7.3: Transmission electron micrographs illustrating carbide formation at both the grain a) and lath b) boundaries in a specimen tempered for 15 minutes at 700°C.

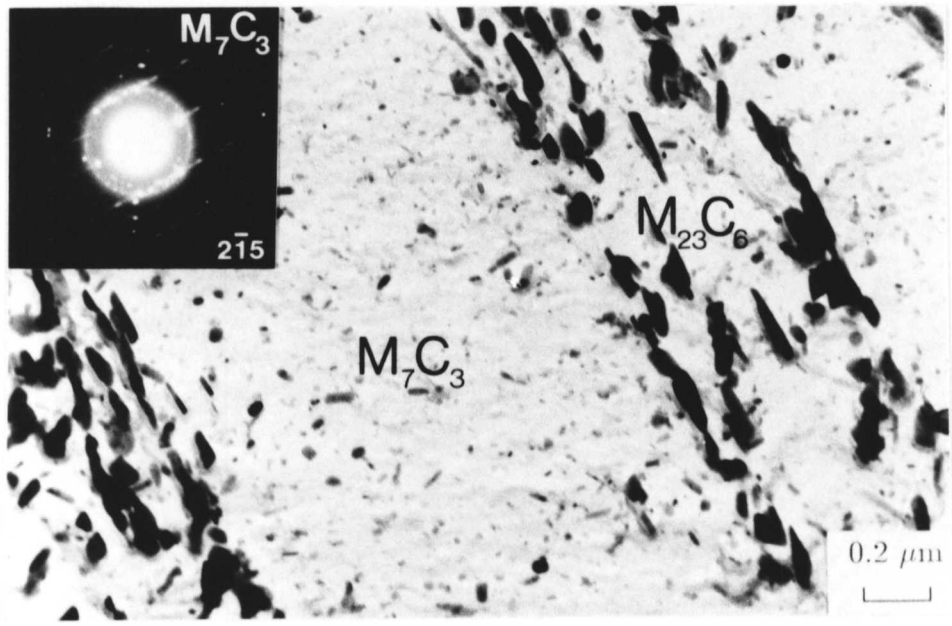

Figure 7.4: Carbon extraction replica showing small M_7C_3 particles distibuted within the martensite laths and distant from the larger $M_{23}C_6$ particles clustered on the lath boundaries. The inset is a selected area diffraction pattern of M_7C_3, the zone axis being $[2\bar{1}5]$ and showing characteristic streaks.

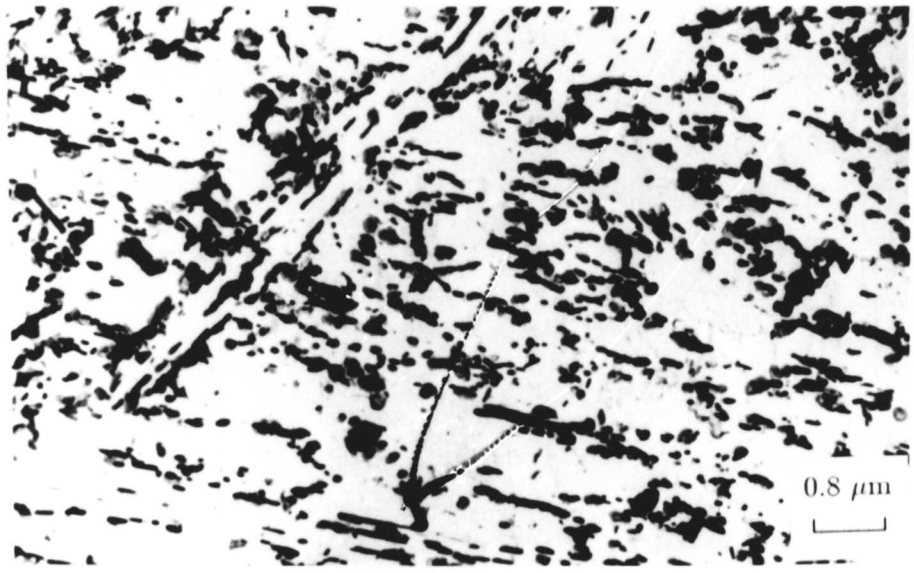

Figure 7.5: Carbon extraction replica from a specimen tempered for 2 hours at 700°C illustrating the distribution of $M_{23}C_6$ carbides with respect to martensite lath boundaries.

a)

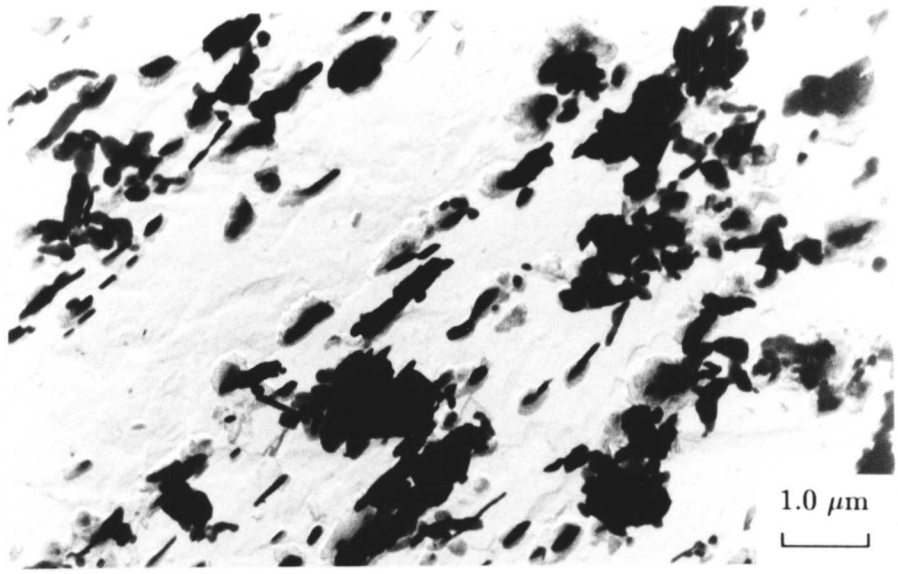

b)

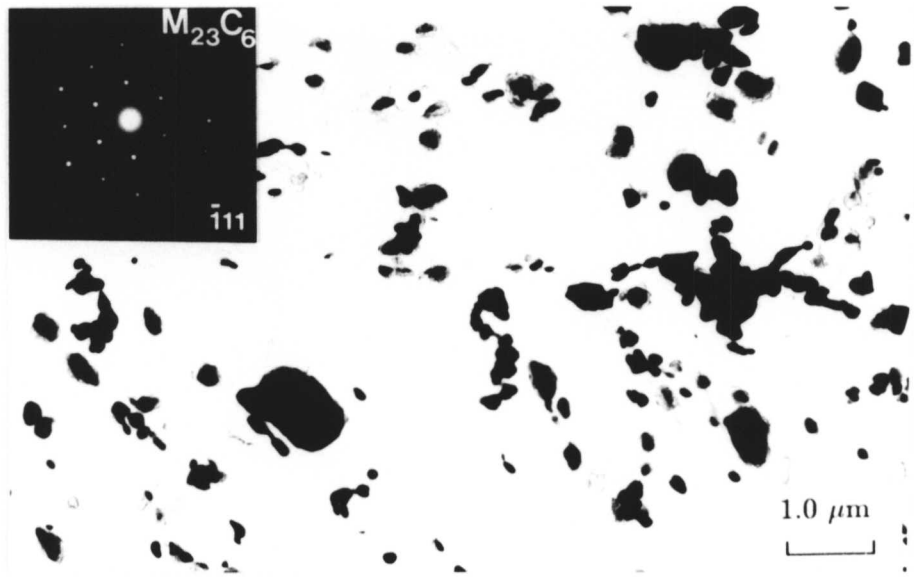

Figure 7.6: A comparison between the distribution of $M_{23}C_6$ carbides in the ex–service material a) and in the specimen isothermally heat treated for 1173 hours at 700°C b) which represent comparable heat treatments according to the empirical Larson–Miller parameter. The inset in figure b) is a selected area electron diffraction pattern of $M_{23}C_6$ in the $[\bar{1}11]$ orientation.

The carbides found in the microstructural investigation were M_7C_3 and $M_{23}C_6$, in good agreement with the sequence predicted by thermodynamic calculations. The EDXS results show that the equilibrium chromium content of the carbide M_7C_3 is higher than that in $M_{23}C_6$. The absolute levels of Cr and Mo predicted to be in the carbides are slightly higher than those observed experimentally (e.g. 65 wt.% Cr and 20 wt.% Mo are predicted in $M_{23}C_6$, whereas 60 wt.% Cr and 10 wt.% Mo, allowing for 5 wt.% C, are measured experimentally), however, there is good general agreement. The chromium content of both carbides in the ex–service material is larger due to the increased bulk chromium content of the alloy. The carbides can support a greater substitutional alloying content as the temperature is lowered. It is possible, therefore, that when the steel is in service at the lower temperature of 565°C, after the stress–relief heat treatment, the chromium content of the $M_{23}C_6$ may increase by approximately 4–5 wt.%. It is likely, however, that this approach to equilibrium will be extremely slow and difficult to detect within the experimental error of energy–dispersive X–ray spectroscopy.

7.3.3 Cementite precipitation

It is interesting to note that no cementite was found in any of the specimens, even during the earliest stages of tempering, because cementite is usually expected to be the first carbide to form on tempering martensite. Therefore the computer model described in Chapter 3 was used to investigate the time for cementite, with an initial composition determined by assuming a paraequilibrium transformation mechanism, to reach its predicted equilibrium composition. The results of these calculations are presented in Figure 7.8. The chromium concentration in the cementite is plotted against the time allowed for diffusion at 700°C for a range of particle sizes between 10 and 30 nm. It can be seen that cementite in fact saturates in an extremely short time, of the order of a few minutes. It is concluded that with the large amount of chromium in the base composition of the steel, the driving force for alloy carbide precipitation is large, and that cementite will only be seen in this steel if tempering takes place at a much lower temperature, or possibly immediately after tempering has begun.

7.3.4 X–ray microanalysis

Extensive measurements of carbide composition and particle size were performed on carbon extraction replicas using EDX. The results of the analyses on the carbides contained in specimens tempered at 700°C for 15, 30, 60 and 120 minutes respectively are presented in Figure 7.9a)–d) as plots of the chromium concentration against particle size, measured in terms of a mean linear intercept.

It can be seen in the 15 minute specimen that M_7C_3 (with a composition of approximately

a)

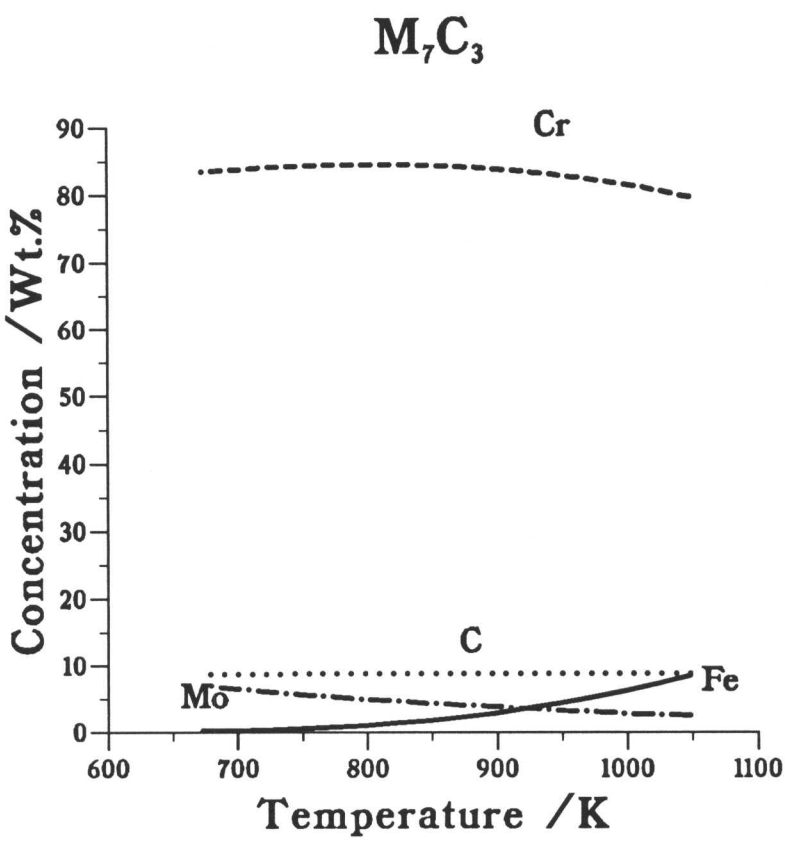

b)

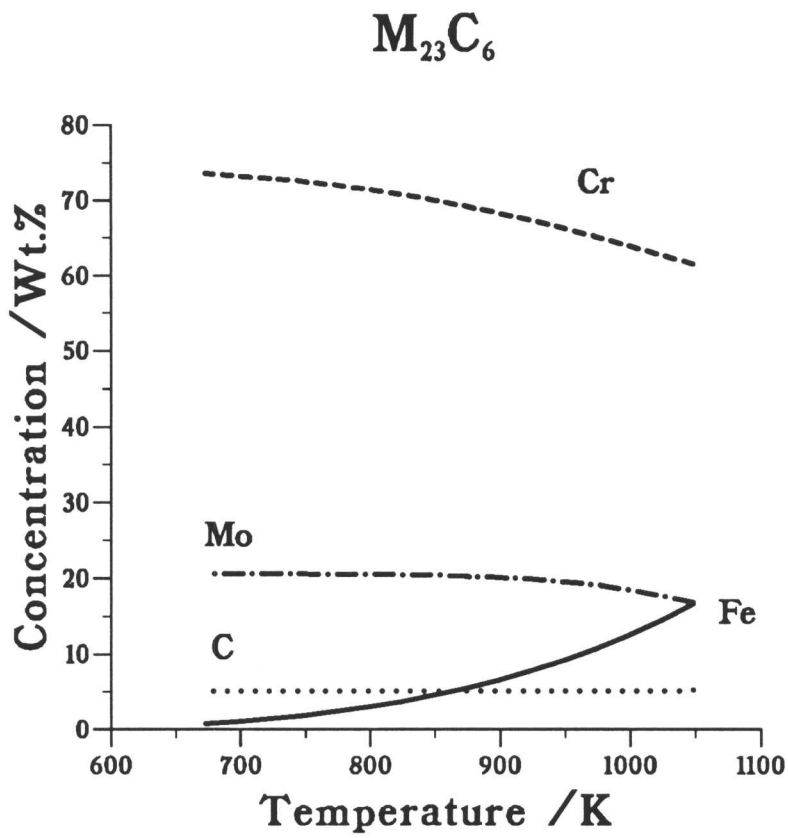

Figure 7.7: Alloying element content of M_7C_3 a) and $M_{23}C_6$ b) carbides as a function of temperature in the 12Cr1MoV steel.

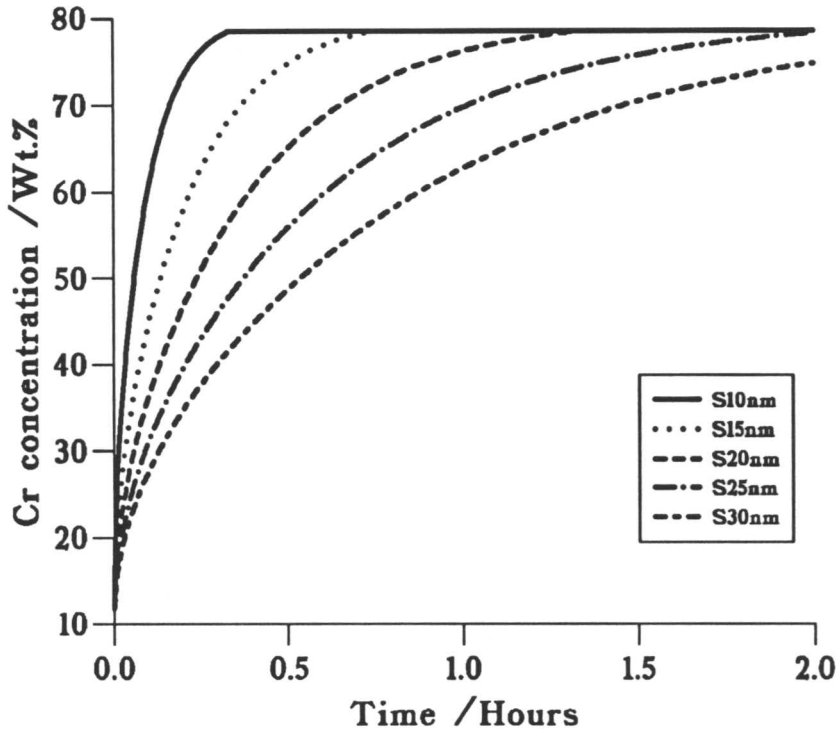

Figure 7.8: Calculated rate of cementite enrichment with respect to chromium concentration for particles of sizes 10–30 nm using a finite difference model.

75 wt.% Cr, 20 wt.% Fe and small amounts of molybdenum and manganese) is found to co–exist with $M_{23}C_6$ (with a composition of approximately 60 wt.% Cr, 30 wt.% Fe and 10 wt.% Mo). These compositions are in general agreement with those of Beech and Warrington (1966), the absolute values being dependent on the base composition of the steel. The average chromium concentration in $M_{23}C_6$ in all the specimens ranged from 60–63 wt.%. The transition from M_7C_3 to $M_{23}C_6$ is picked up in the 30 minute specimen. After 1 hour there is very little evidence of any M_7C_3 being present in the microstructure, and after the completion of the stress–relief heat treatment all the M_7C_3 has redissolved. Figure 7.9e) compares data from the 'ex–service' material and the specimen tempered for 1173 hours at 700°C. The chromium content in the carbides in the 'ex–service' material is larger than that in the isothermally tempered specimen, but this difference can be attributed to the the higher chromium content in the base composition of the steel and the longer tempering time. In both cases, however, the chromium content is constant.

7.3.5 X–ray diffraction analyses

X–ray diffraction analyses on particles extracted from the steel matrix using the method described in Chapter 4 for specimens tempered at 700°C for 10 minutes and 2 hours respectively

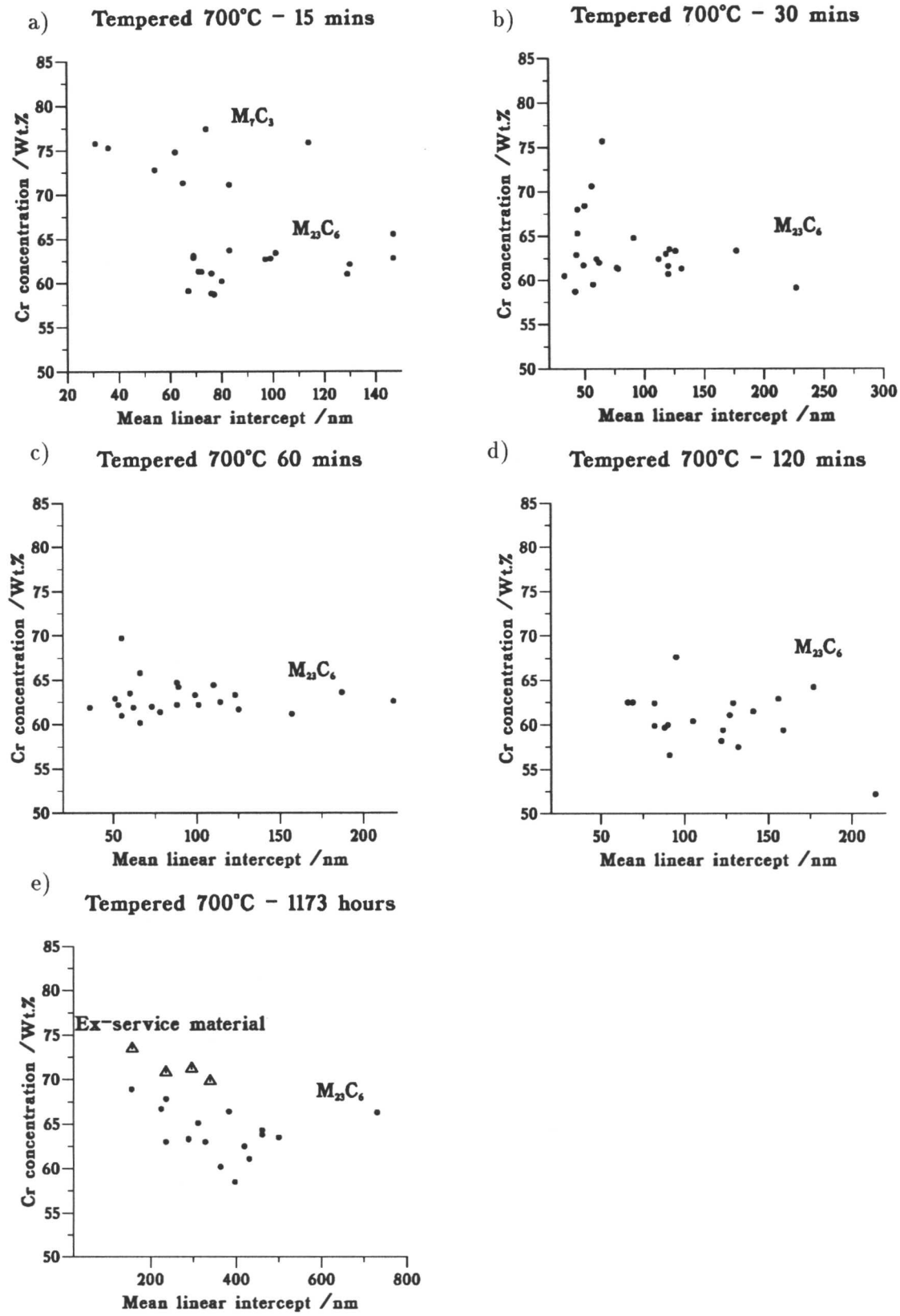

Figure 7.9: a)–e) Cr concentration versus particle size for specimens tempered at 700°C for varying times. In e) the results are compared with the composition of $M_{23}C_6$ in the ex–service material.

are presented in Figure 7.10a) and b). In the spectra for the specimen tempered for 10 minutes, the 420 and 202 peaks from M_7C_3 are clearly visible, whereas these have disappeared after tempering for 2 hours. The 420 and 202 peaks are the strongest visible peaks for M_7C_3 because the strong 421 peak overlaps with the strong 511 peak of $M_{23}C_6$. There was no further change in the diffraction pattern for specimens tempered up to 1200 hours at 700°C. The lattice parameters for $M_{23}C_6$ extracted from all the heat–treated specimens of the 12Cr1MoV steel were calculated using the measured values of d–spacings. Errors can arise in the measured values of the d–spacings factors such as the geometry of the diffractometer and absorption in the specimen. These were corrected for by fitting a polynomial function to the d–spacings of the internal standard, which are known to a high degree of accuracy. $M_{23}C_6$ is cubic and therefore the d–spacings and plane indices are related by the equation

$$d_{hkl}^2 = \frac{a^2}{h^2 + k^2 + l^2}.$$

The adjusted d–spacings were fitted to this equation using a non–linear least–squares procedure. The calculated lattice parameters are presented in Table 7.4.

Table 7.4: Lattice parameters of $M_{23}C_6$ determined by X–ray diffraction.

Time at 700°C	Lattice parameter /Å
10 mins	10.64± 0.01
15 mins	10.65± 0.01
30 mins	10.66± 0.01
1 hour	10.65± 0.01
2 hours	10.65± 0.01
1173 hours	10.66± 0.01
2 hours +	10.65± 0.01
16 hrs at 565°C	

The lattice parameter of $(Fe, Cr)_{23}C_6$ containing 60 wt.% Cr extracted from a commercial steel containing 14 wt.% Cr has previously been measured as 10.595Å (Gullberg, 1971). In order to estimate the change in lattice parameter due to the molybdenum content in the $M_{23}C_6$ in this work the relative sizes of the atoms are considered. Molybdenum atoms are 10% larger than chromium and may replace up to 8 out of 92 of the metal atoms in the unit cell (Franck *et al*, 1982). The 10 wt.% Mo measured in the carbide corresponds to $Cr_{16}Fe_6Mo_1C_6$, and therefore an increase in lattice parameter to $10.59(1+0.1\times\frac{1}{23})$=10.64Å is predicted. This is

a)

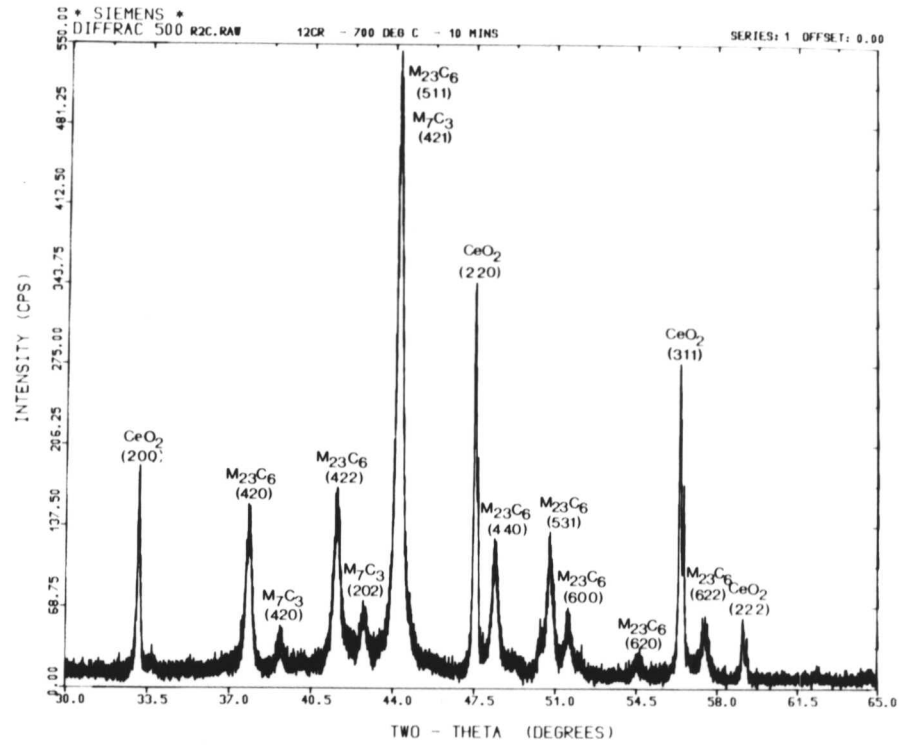

b)

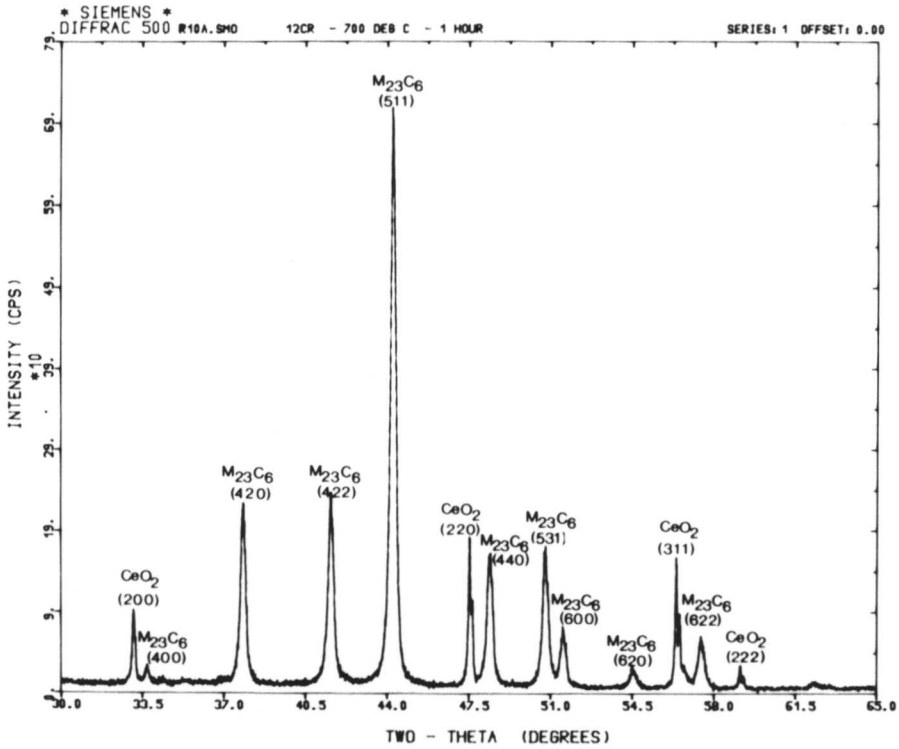

Figure 7.10: X–ray diffraction patterns for specimens tempered at 700°C for 10 mins a) and 1 hour b) respectively illustrating that M_7C_3 initially present along with $M_{23}C_6$ has dissolved after tempering for 1 hour.

in good agreement with the calculated value. The calculated lattice parameters differed by no more than 0.02Å, indicating again no significant differences in the composition of the $M_{23}C_6$ after tempering.

7.4 Discussion

The carbides precipitating during the stress–relief heat treatment in 12Cr1MoV steel have been identified by X–ray diffraction and selected area electron diffraction as M_7C_3 and $M_{23}C_6$. Therefore, before entering service at approximately 565°C, the steel contains a distribution of $M_{23}C_6$ particles. The initial composition of the carbides is close to that predicted using equilibrium thermodynamics, and it has been established by EDX that there is no further change in the composition of the carbides with tempering. No significant dependence of chromium concentration on particle size was found. Lattice parameter measurements and comparison with ex–service material confirm that there is no change in composition of the $M_{23}C_6$ on tempering, especially with respect to molybdenum, which might have been expected from the thermodynamic calculations. The fact that there is no enrichment occurring on tempering in 12Cr1MoV steel is in contrast to the low alloy steels reported in the previous chapter. Du (1986) found that the chromium content in $M_{23}C_6$ precipitating in a $\frac{1}{2}Cr\frac{1}{2}Mo\frac{1}{4}V$ steel increased with time. Whether or not alloy carbides precipitate at their equilibrium composition is therefore dependent on the concentration of alloying elements available in the base composition of a steel. Recent work by Bjärbo (1991) (for an alloy with a higher chromium content than that used in this work) has shown that $M_{23}C_6$ which precipitates during the stress–relief heat treatment is enriched in chromium by less than 5 wt.% during a creep test for 20,000 hours at 600°C.

7.5 Conclusions

The kinetics of carbide precipitation in 12Cr1MoV steels are rapid when compared with other low–alloy steels of the type commonly used in power plant. This is attributed to the fact that the steel studied has relatively large concentrations of carbide–forming substitutional solutes. Thus, unlike the low–alloy steels, relatively stable alloy carbides have been found to dominate in the microstructure immediately after the stress–relief heat treatment. Since this heat treatment is always necessary before implementing the alloy in service, there seems little prospect of estimating the thermal history of a component from the chemical composition of its carbides. In fact, both the thermodynamic analysis and the experimental data show that the chromium concentration of the $M_{23}C_6$ carbide is very sensitive to the average chromium concentration of the steel. It is found that variations in the chromium concentration within

the accepted industrial specifications, can lead to larger corresponding variations in carbide compositions, than would be caused during service.

It has been established that there is no significant change in the carbide identity or composition during service after the stress–relief heat treatment. Therefore, the question arises as to which other microstructural changes could be fruitfully investigated. It seems from a comparison of figures 7.9d) and e), which show an increase in particle size from about 125–300 nm, that carbide coarsening could potentially be used as a microstructural parameter.

CHAPTER 8

ATOM PROBE AND STEM INVESTIGATIONS

The atom probe studies discussed in this chapter provide a link between the experimental measurements of mean concentration levels in cementite using energy dispersive X–ray analysis in a transmission electron microscope, and the theoretical modelling of the diffusion process discussed in Chapter 3. Consistent with theoretical predictions, the enrichment of substitutional solutes in the carbide at the carbide/matrix interface is not observed to reach the levels required for local equilibrium at the interface.

The material described in this chapter has been accepted for publication in Surface Science.

CHAPTER 8

ATOM PROBE AND STEM INVESTIGATIONS

8.1 Introduction

It was shown in Chapter 3 that the cementite associated with upper bainite forms with no redistribution of the substitutional alloying elements, by paraequilibrium transformation. The modelling of the subsequent approach towards equilibrium, involving the diffusion of substitutional elements is central to this work. It is often assumed in problems of diffusion that local equilibrium exists at an interface. † A calculation was performed using MTDATA (see Chapter 3) to determine the equilibrium concentration of chromium in cementite and ferrite for the $2\frac{1}{4}$Cr1Mo steel at 565°C. Alloy carbide formation was suppressed; only the phases cementite and ferrite were allowed to exist. The results of the calculation are given in Table 8.1. The predicted volume fraction of cementite at this temperature was 0.022, which is consistent with mass balance considerations. The partitioning ratio indicated by the calculations is consistent with the values of $\simeq$50 measured by Al–Salman *et al* (1979) at 600°C for pearlitic cementite in an Fe–Cr–Mn–C steel, although this comparison is not strictly valid because of the difference in steel chemistry. Local equilibrium therefore would require a very large increase in chromium concentration in cementite at the interface, compared with the 2.2 wt.% that exists in the bulk alloy.

Table 8.1: Calculated equilibrium concentration in cementite and ferrite at 565°C.

	Calculated equilibrium concentration of Cr /wt.%
Ferrite	1.05
Cementite	54.00

Modelling of the enrichment behaviour of cementite to date assumes only that local equilibrium exists in the *matrix* at the carbide/matrix interface. The concentration in cementite at the interface is determined by mass balance considerations in the diffusion equations. During the earlier stages of enrichment (*e.g.* 10 mins) the model predicts a small increase in the concentration of chromium at the edges of a cementite particle with respect to its core. At the

† Local equilibrium requires that the concentrations of the solute in both the carbide and the matrix at a carbide/matrix interface are given by the tie–line of the equilibrium phase diagram.

longer tempering times, after soft impingement of the diffusion fields from the extremities of the particle, the model predicts a more even distribution of chromium across the particle rising slowly to the equilibrium level. Measurements of cementite composition using energy–dispersive X–ray analysis (EDX) in a TEM are only able to determine the average particle concentration. The maximum measured Cr concentration in cementite by EDX in the specimens tempered at 565°C was $\simeq$ 35 wt.%. It is not possible to measure the equilibrium Cr content in the cementite in this steel at this temperature because the alloy carbide M_7C_3 precipitates at the expense of the cementite before it has reached saturation.

The model assumes that the diffusion coefficients, D_α and D_θ, in the matrix and cementite respectively are the same; this assumption is justified to some extent by the good agreement between kinetic theory and experiment demonstrated in Chapters 5, 6 and 7. D_α is obtained as $1.65\times10^{-19}m^2s^{-1}$ according to Fridberg *et al* (1969), whose assessed data are in good agreement with those of Bowen and Leak (1970). Barnard *et al* (1987) have used atom probe techniques to measure D_α and D_θ. The data for 486°C are presented in Table 8.2. The value of D_α measured by Barnard *et al* is an order of magnitude less than the other two values, and of D_θ approximately two orders of magnitude less than the measured value of D_α.

Table 8.2: Measurements of the diffusion of chromium in ferrite and cementite at 486°C.

	D_α/m^2s^{-1}	D_θ/m^2s^{-1}
Bowen and Leak (1970)	4.9×10^{-21}	–
Fridberg *et al* (1969)	4.6×10^{-21}	–
Barnard *et al* (1987)	(1) 2.6×10^{-22}	–
	(2) 4.9×10^{-22}	0.02×10^{-22}

The effect of varying the value of D_θ with respect to the value of D_α on the cementite enrichment rate was therefore investigated using the model described in Chapter 3. Three different values of D_θ were chosen and two different tempering times, 10 mins and 178 hours. The resulting composition profiles and predicted concentrations are presented in Figure 8.1 and Table 8.3. The most important result is that for $D_\theta = \frac{1}{50} D_\alpha$ the predicted average level of Cr in cementite is 16 wt.% for a 10 min ageing period, whereas if $D_\alpha = D_\theta$ this level is 2.5 wt.%. The average concentration of chromium in cementite after 10 mins tempering measured using EDX is $\simeq$6 wt.%. This result is therefore inconsistent with the value of D_θ measured by Barnard *et al* (1987). It is possible that D_θ is slightly less than D_α, but not by a factor of 50.

The purpose of this work was therefore to investigate to what extent local equilibrium exists at the particle/matrix interface during the enrichment of cementite.

Table 8.3: Average Cr concentration and the interface concentration in cementite as a function of D_θ and tempering time. Concentrations are given in wt.%.

D_θ	10 mins		178 hours	
	Av. conc.	Interface conc.	Av. conc.	Interface conc.
$=D_\alpha$	2.48	3.14	13.09	13.11
$=0.3D_\alpha$	3.14	5.23	38.51	38.59
$=0.02D_\alpha$	16.06	47.74	53.99	53.99

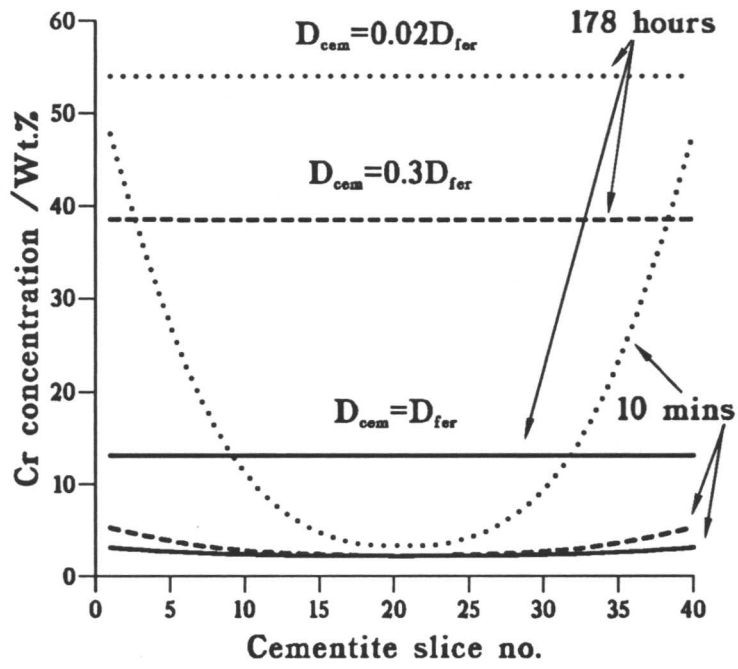

Figure 8.1: Predicted chromium concentration in a cementite particle of size 100 nm in a $2\frac{1}{4}$Cr1Mo steel after 10 mins and 178 hrs tempering at 565°C as a function of the diffusion coefficient in cementite. Slices 1 and 40 represent the surfaces of a plate–shaped cementite particle in the finite difference model, the core being located at slice 20.

8.2 Atom probe field ion microscopy

8.2.1 Principle of operation of atom probe

An atom probe consists of a field ion microscope with an ultrahigh–resolution mass spectrometer attached. The field ion microscope produces images of the specimen in which there is one–to–one correspondence with atomic positions. The mass spectrometer is then used to

perform very accurate chemical analysis. A brief summary of the principle of operation of an atom probe is presented below. Extensive discussion concerning the operation of atom probes can be found in the book by Miller and Smith (1989), and details of the atom probe used in this work in the paper by Waugh *et al.* (1992).

A field ion specimen is a very sharp needle of tip radius approximately 100 nm. The specimen is cooled down to cryogenic temperatures using a closed–cycle helium refrigerator and held in a vacuum chamber with a background pressure of 10^{-11} mbar. For producing a field ion image (*field ionisation*), a background pressure of neon gas of 10^{-5} mbar is introduced into the chamber and a large positive voltage is applied to the specimen. The inert gas atoms become polarised in the high electric field near the tip and are attracted towards it. Ionisation of the polarised gas atom can then occur by quantum mechanical tunnelling of an electron to the tip. The remaining positively charged gas ion is then repelled from the tip towards the channel plate. On striking the channel plate, a cascade of electrons is produced which strike a phosphor screen resulting in a bright image spot. The number of ions will be greatest where the local field is highest, for example, above prominent surface atoms. A picture of the Cambridge atom probe is presented in Figure 8.2, and the corresponding schematic diagram in Figure 8.3.

Limited information can be obtained from the field ion image. The image is usually used to recognise features of interest such as second phases or boundaries. Phase contrast can arise where there are differences in the ionisation probabilities of the elements in the two phases. Ferrite is usually imaged as sets of concentric rings showing the b.c.c. symmetry of the phase, whereas austenite, martensite and carbides usually image darkly. The elements molybdenum and silicon, to a lesser extent, image brightly because the evaporation field for these elements from an iron–based matrix is higher than that for iron itself, and so they remain at prominent surface positions.

The second stage involves the removal of atoms from the surface of the specimen by the process of *field evaporation* as the voltage applied to the specimen is increased further. The background pressure of neon gas is reduced for atom probe analysis. The atoms are field–evaporated at a well–defined moment in time by the application of an additional voltage pulse. The mass to charge ratio of the atom can then be determined from the time taken to reach the detector, which can be measured to an accuracy of 1 ns. There is a hole in the channel plate which enables the selection of atoms from a specific area. The lateral resolution is the size of this hole projected onto the tip, which is approximately 5 nm. The accuracy with which small scale composition variations can be determined depends on their relative orientation to the axis of the analysis cylinder. Repeated pulsing of the sample is used to build up a layer by layer

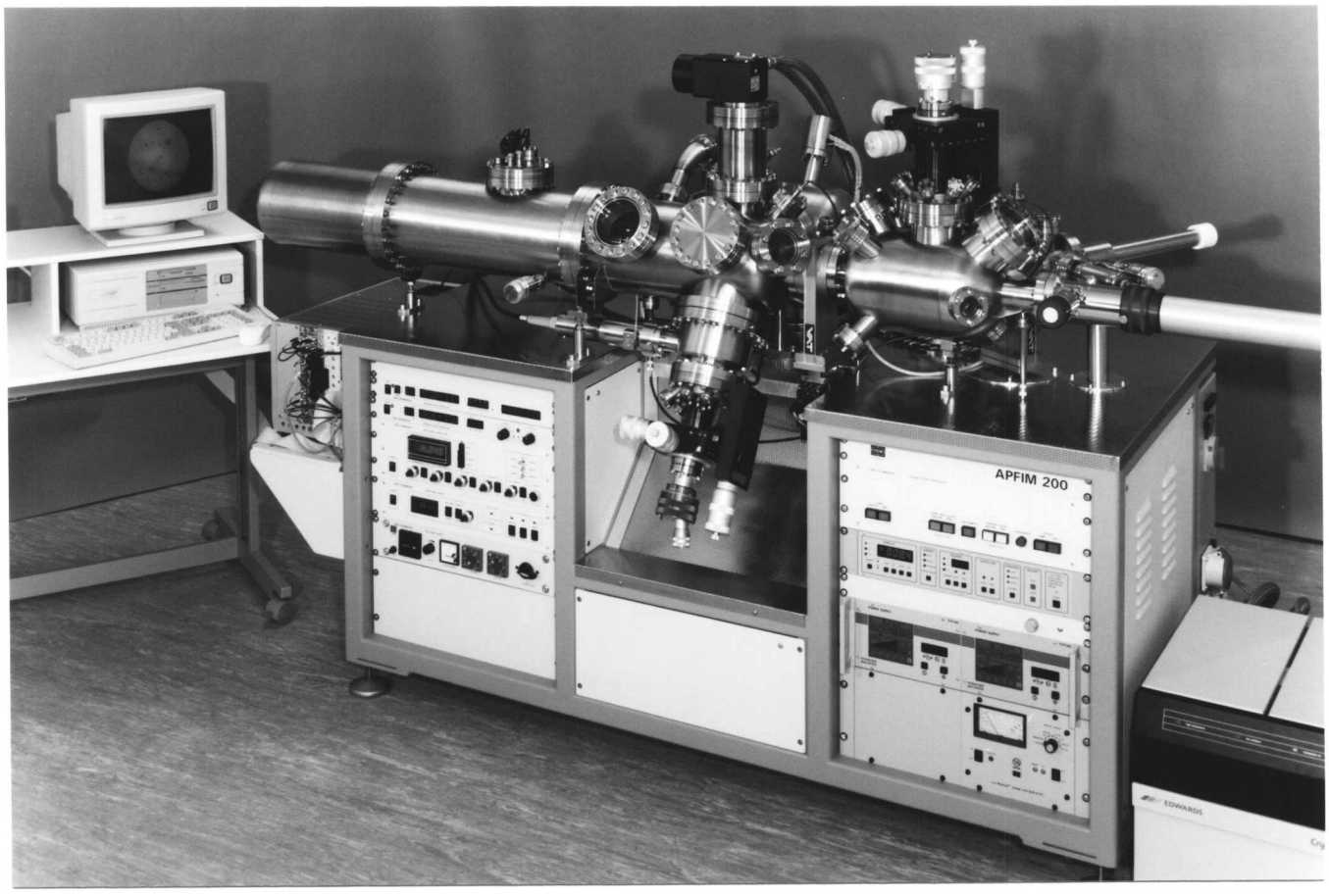

Figure 8.2: The atom probe field ion microscope (APFIM 200) used in this work.

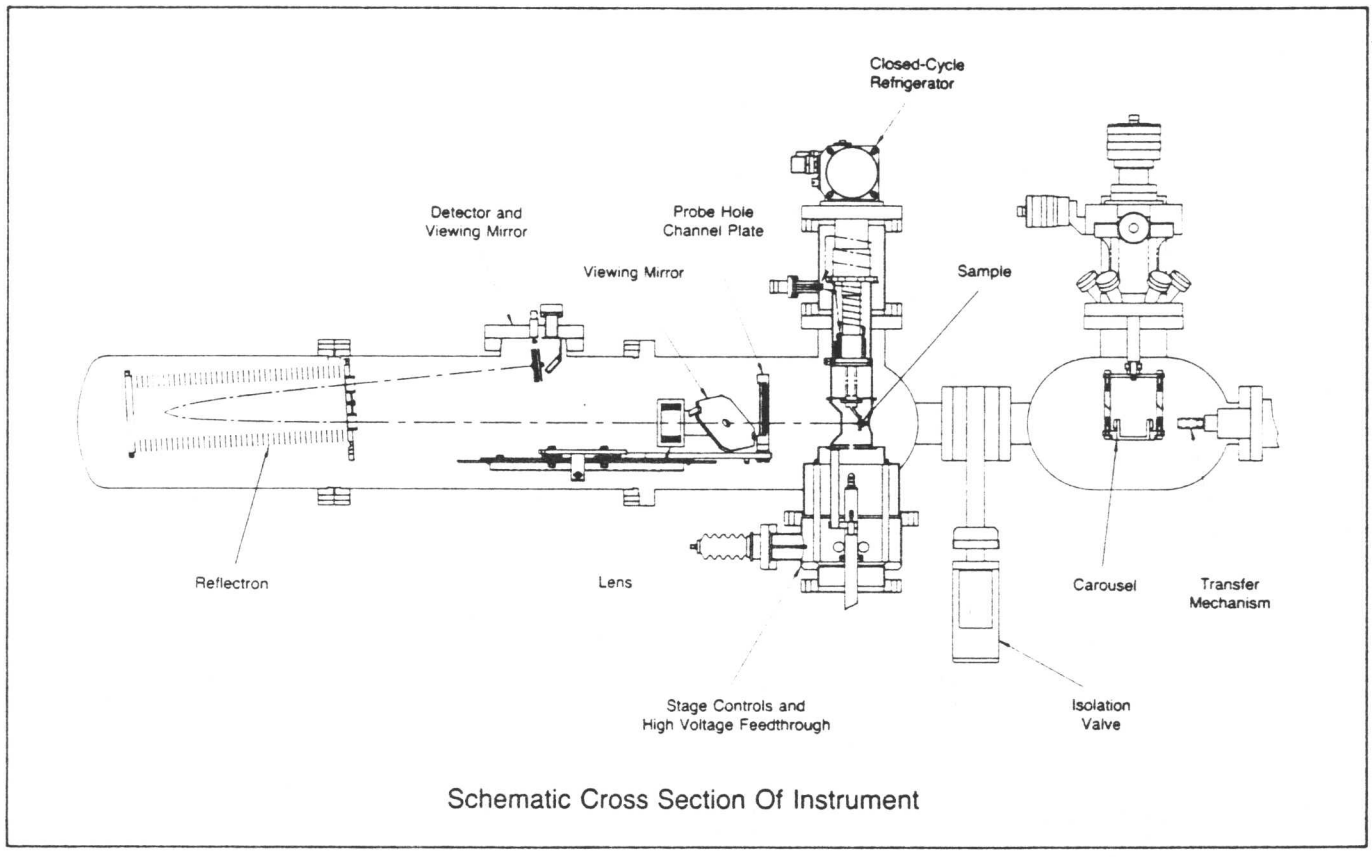

Figure 8.3: A schematic cross section of the APFIM 200.

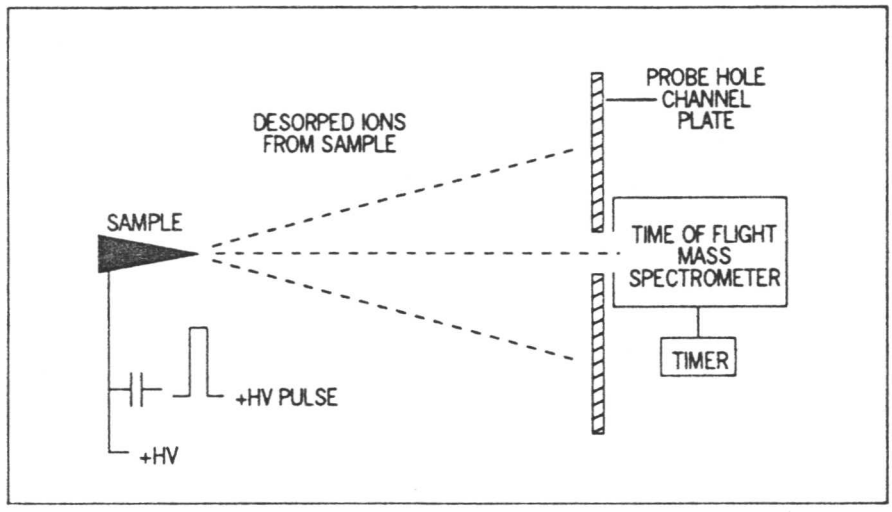

Figure 8.4: Schematic diagram illustrating the operation of the atom probe field ion microscope.

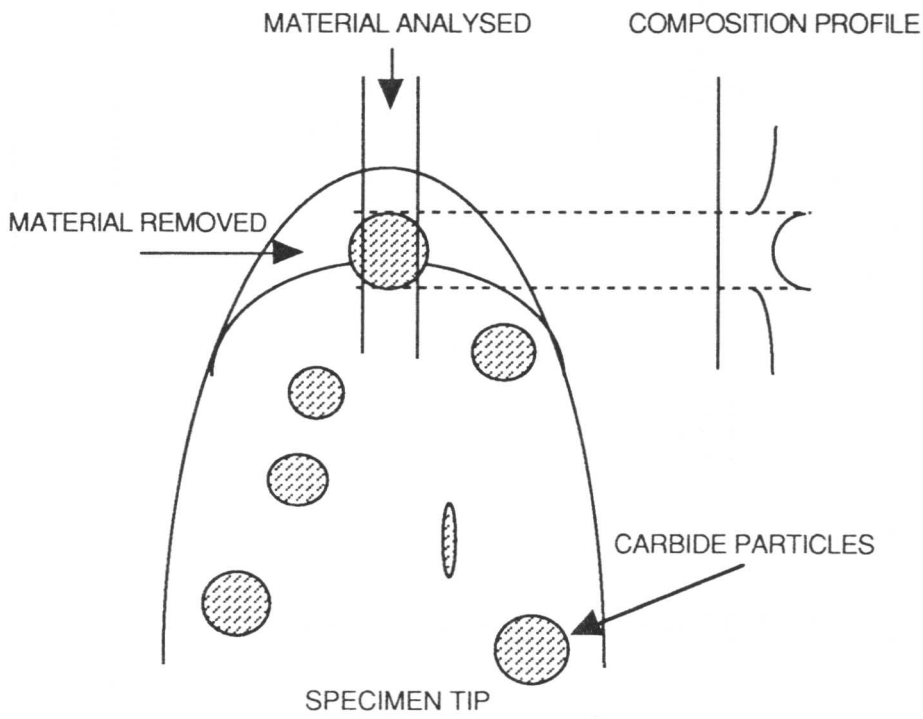

Figure 8.5: Diagram illustrating the ideal precipitate analysis geometry.

atomic composition profile from the specimen. A schematic diagram illustrating the operation of the atom probe field ion microscope is presented in Figure 8.4. A diagram illustrating the ideal precipitate analysis geometry is illustrated in Figure 8.5.

8.2.2 Experimental details

The $2\frac{1}{4}$Cr1Mo steel discussed in chapter 5 was used for the atom probe studies. Blanks were cut from the heat treated specimens of size 0.5×0.5×20 mm using a diamond saw. These were initially thinned electrochemically using the same conditions as for the preparation of the TEM foils of this material discussed in chapter 4. Needles for examination in the atom probe were then prepared using a two stage electropolishing technique; stage 1 producing a necked specimen profile using a thin layer of the electropolishing solution above floated on an inert solution at ≃30 V, and stage 2 producing a needle by electropolishing in a solution of 2% perchloric acid in butoxyethanol at ≃25 V. Both solutions were cooled to 0°C using liquid nitrogen. Specimens were resharpened by dipping the tips in a lacquer resist and electropolishing in the two solutions. Atom probe analyses were performed at 100 K with background pressures of neon gas of 1×10^{-5} mbar and 1×10^{-8} mbar for imaging and analysis respectively. The voltage pulse fraction used was 20%.

8.2.3 Results and discussion

The specimens tempered for relatively short times (up to 2 hrs) were examined in the atom probe, and those for longer times in the STEM, which was able to accommodate the larger particle sizes. A typical TEM micrograph from a thin foil tempered for 10 mins at 565°C is shown in Figure 8.6, showing plate–shaped carbides, identified as cementite using selected area electron diffraction. The cementite plates typically measured 125×30 nm. Analysis in the atom probe is easier if the particles are aligned with the long dimension parallel to the length of the needle. As observed by Wada *et al.* (1982), the cementite particles were found to be very unstable under the action of the applied electric field, leading to frequent specimen fracture. It was observed in the STEM that the cementite particles charged in the electron beam indicating poor conductivity.

Field ion micrographs from the matrix and cementite phases are presented in Figure 8.7. The image from the matrix was often found to contain small clusters of very bright atoms; subsequent atom probe analysis showed that these might be attributed to very small molybdenum carbides. The cementite phase is observed to have little structure in the image and to contain relatively large diffuse spots.

Mass spectra from specimens tempered for 10 mins and 2 hrs are presented in Figure 8.8.

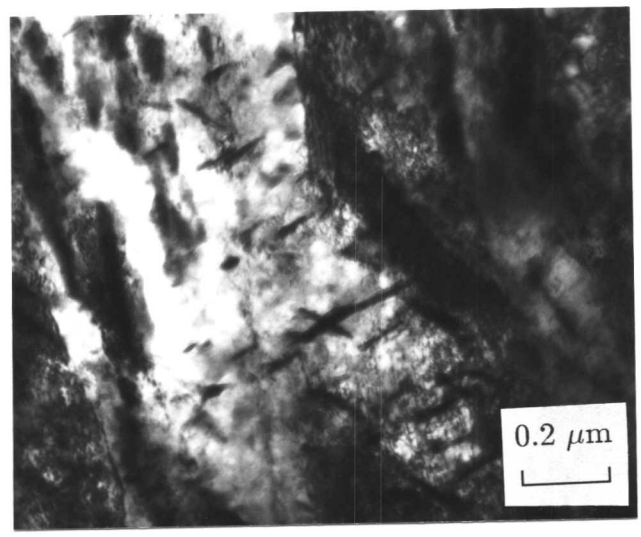

Figure 8.6: A transmission electron micrograph from a specimen tempered at 565°C for 10 mins illustrating plate–shaped cementite particles.

a)

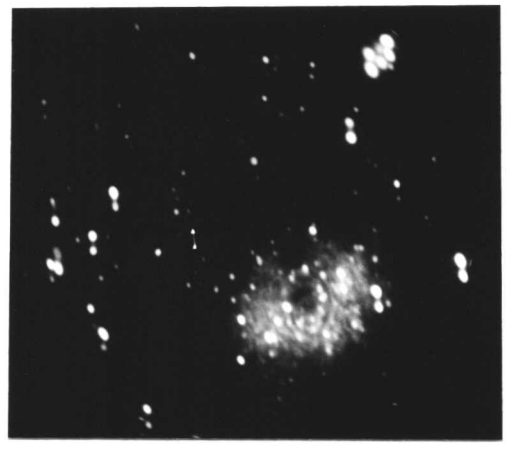

b)

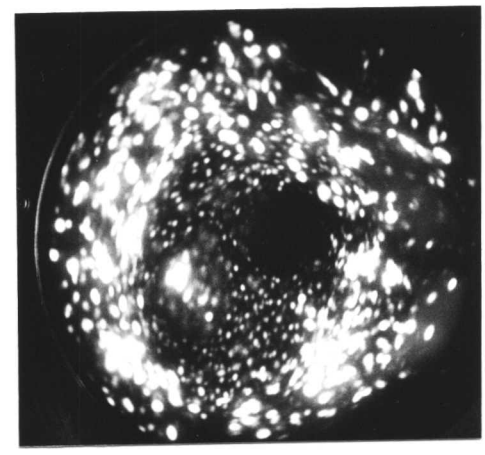

Figure 8.7: Field ion images from the matrix (a) and the cementite (b) phases.

The calculated composition within the matrix, distant from the cementite particles, corresponding to each of these spectra is presented in Table 8.4. It can be seen that there is a reduction in the chromium level in the matrix after tempering for 2 hrs. This corresponds to the enrichment of cementite with respect to chromium, resulting in a drop in the chromium level in the matrix. After 2 hrs tempering, the concentration of chromium measured in cementite by energy–dispersive X–ray analysis on carbon extraction replicas in the TEM is approximately 11 wt.%.

It is interesting to note that the molybdenum and carbon contents in the matrix are a little higher than might be expected, particularly in the specimen tempered for 10 mins. Close examination of the composition profile corresponding to the mass spectrum in Figure 8.9a) reveals small clusters containing both molybdenum and carbon atoms. This is illustrated in Figure 8.9a). This suggests there are very small particles of molybdenum carbide in the early stages of formation within the matrix. A Markov chain analysis for the the molybdenum atoms indicates that there are more Mo–Mo bonds than would be expected in a homogeneous solid

Table 8.4: Composition of the matrix measured in the atom probe for samples tempered for 10 mins and 2 hrs in wt. %.

Time	C	Si	Mn	P	S	Cr	Mo	V	Ni	Cu	Fe
10 mins	0.16 ±0.02	0.49 ±0.06	0.48 ±0.08	0.01 ±0.01	0.04 ±0.01	2.38 ±0.15	1.87 ±0.20	0.09 ±0.03	0.09 ±0.02	0.03 ±0.03	94.36 ±0.60
2 hrs	0.13 ±0.03	0.37 ±0.07	0.60 ±0.14	0.05 ±0.03	–	1.34 ±0.20	1.04 ±0.25	–	0.04 ±0.04	–	96.44 ±0.75

(a)

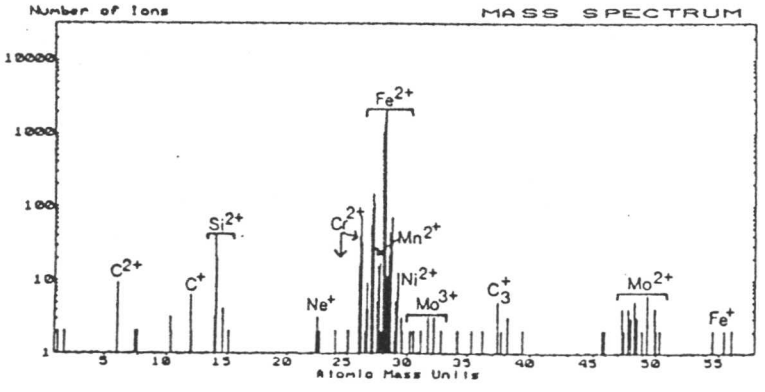

(b)

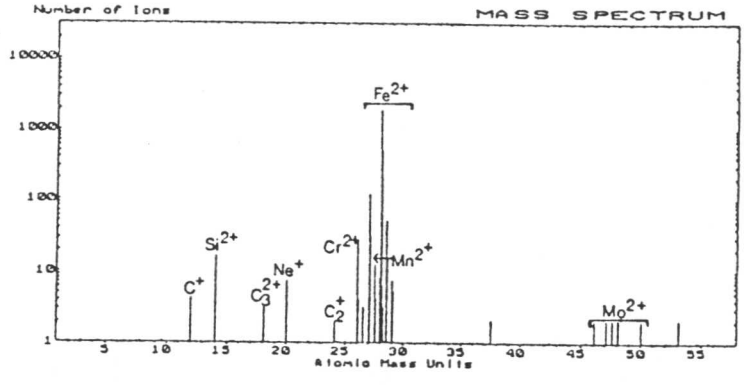

Figure 8.8: Mass spectra taken from the matrix in specimens tempered for 10 mins (a) and 2 hrs (b) containing 7,000 and 3,000 ions respectively.

solution, although many more ions are needed to establish the significance of this result. Further work is therefore needed to establish any correlation between the carbon and molybdenum concentrations, and to examine the development of clusters as a function of ageing time. Similar

observations have been made by Olson *et al.* (1991). Dark field imaging in the STEM at high magnification, which is especially good for showing high atomic number contrast, is able to resolve small particles which probably correspond to the molybdenum and carbon clusters observed in the atom probe. This is illustrated in Figure 8.9b). Mo_2C particles had not been observed in previous TEM investigations until the specimens had been tempered for 32 hrs.

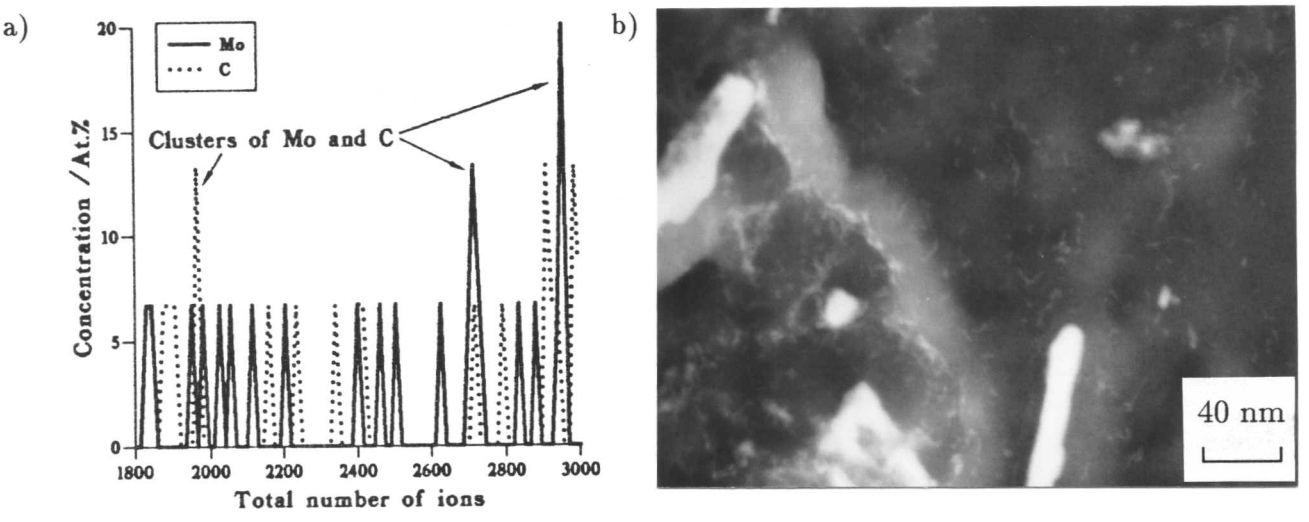

Figure 8.9: a) Composition profile (15 ions per block) corresponding to part of the mass spectrum in Figure 8.9a) for the specimen tempered for 10 mins showing small clusters of molybdenum and carbon atoms and b) dark field STEM micrograph from a carbon extraction replica taken from a specimen tempered for 10 mins illustrating very small particles exhibiting high atomic number contrast.

The measured content of silicon in the matrix is observed to be slightly higher than the composition of the steel as a whole. Silicon, usually observed as Si^{2+}, has a mass to charge ratio of 14, which is the same as that for N^+. However, the concentration of nitrogen in the steel is expected to be less than 40 ppm. High levels of Si is a common observation, and is usually attributed to the preferential evaporation of the matrix because Si is refactory and hard to evaporate. Preferential evaporation occurs because the iron evaporates more easily, so that during the time when the specimen is not being pulsed (*i.e.* is at the set d.c. voltage) the iron continues to evaporate whereas the Si only evaporates during the pulsing. Therefore, the Si appears to have a larger concentration than expected.

A typical mass spectrum from a cementite particle after 10 mins tempering is illustrated in Figure 8.10. The corresponding concentration for the major alloying elements of interest is approximately 20 at.% C, 3 at.% Cr, 2 at.% Mo and the balance, Fe. The chromium and molybdenum levels are slightly lower than those measured by energy–dispersive X–ray analysis ($\simeq$5 at.% Cr), possibly because there is expected to be a variation with particle size. However,

the carbon content is clearly less than the 25 at% required by the stoichiometry of cementite, M_3C. It is possible that the probe hole did not completely overlap the cementite particle, but is more likely that the carbon detection efficiency has been reduced by the relatively high analysis temperature used to try to reduce the fracture rate of the samples. Carinci *et al.* (1988) found that a specimen temperature of 80 K reduced the observation of carbon clusters and led to a corresponding reduction in the overall carbon content. Sha *et al* (1992) have recently shown that there is an ambiguity in the assignment of the peaks due to carbon clusters C_2^+ and C_4^{++} and that careful reassignment of these peaks can increase the total amount of carbon in the atom probe analysis by as much as 10%.

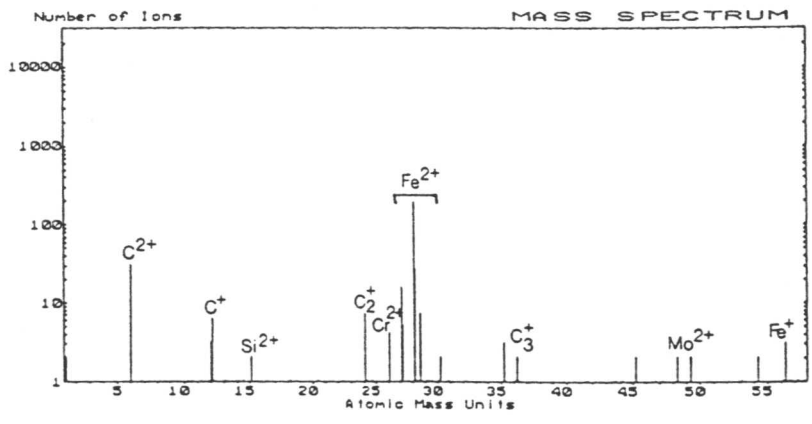

Figure 8.10: A typical mass spectrum from a cementite particle in a specimen tempered for 10 mins.

The composition profiles of carbon, chromium and silicon along a cementite/matrix interface for a specimen tempered for 5 mins are presented in Figure 8.11. The carbon concentration here is only 10 at.%, consistent with the probe hole being half way across the carbide and the matrix. The inclination of the probe hole to the interface was approximately 80°C. It is important to note that the concentration of chromium in the cementite at the interface is far less than the 54 wt.% expected from local equilibrium. This result therefore verifies the theoretical model in which local equilibrium does not exist in the cementite during the early stages of enrichment. There is also some evidence of an increase in the silicon content of the matrix outside the cementite particle. Silicon is known to partition from cementite.

8.3 Scanning transmission electron microscope studies

It has already been noted that atom probe analyses were difficult because of the size of the carbides relative to the size of the specimen tip. After the precipitation of the larger M_7C_3 carbides atom probe analyses proved nearly impossible. Therefore a scanning transmission

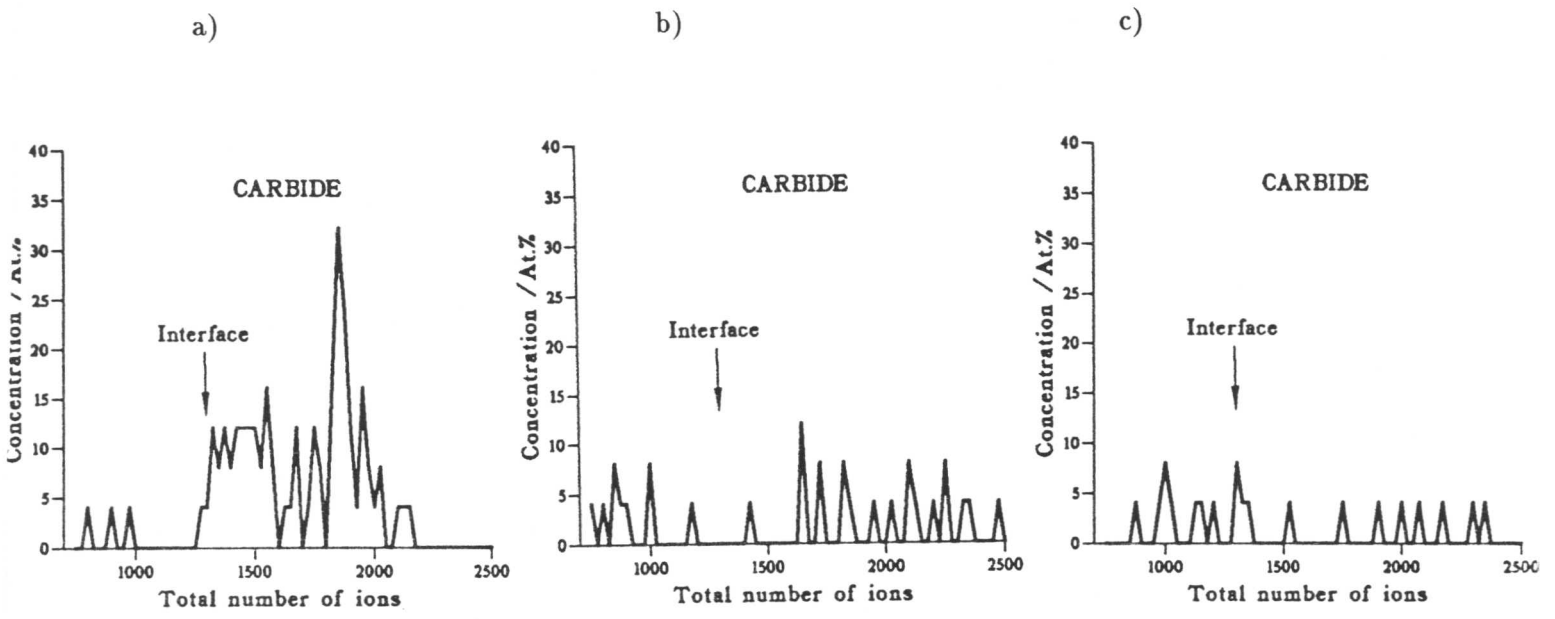

Figure 8.11: Composition profiles for carbon (a), chromium (b) and silicon (c) along a cementite/matrix interface in a specimen tempered for 5 mins.

electron microscope (STEM) was used to look at the composition profile through some of the larger cementite particles. Analyses were performed using a VGHB501 STEM operated at 100 kV on thin foils made from the specimens tempered for 178 hours. A little caution needs to be exercised in the interpretation of these results for two reasons. Firstly, the resolution of the STEM was at its poorest due to a strong astigmatism produced by the ferromagnetic specimen. (Attempts to use carbon extraction replicas proved unsuccessful because the specimen drifted within the time needed to perform accurate microanalysis.) In addition the particle is 3–dimensional; any surface enrichment will be averaged to some extent because the particle is probed by the electron beam in a 2–dimensional section.

8.3.1 Results and discussion

Figure 8.12 shows the chromium concentration profile across a cementite particle and into the matrix measured using energy–dispersive X–ray analysis in a STEM. This particle is contained in a specimen which has been tempered for 178 hours at 565°C. Care has been taken only to include the section of the particle having parallel sides in the analysis in order to remove any interference from the matrix at the ends of the particle. The analysis was performed in a direction exactly normal to the carbide/matrix interfaces. The absolute level of chromium measured in the matrix was lower than that measured on a carbon extraction replica (Chapter 5) due to interference from the predominantly iron–containing matrix. Thus, it is not possible

to determine an absolute level of chromium in the cementite. However, the relative difference between the chromium concentration at the centre and the edge of the particle was found to be approximately 3 wt.%. This result is significant because it would appear to preclude the possibility that the chromium concentration in the cementite at the carbide/matrix interface has reached the predicted equilibrium level, implying local equilibrium has not yet been attained at the interface.

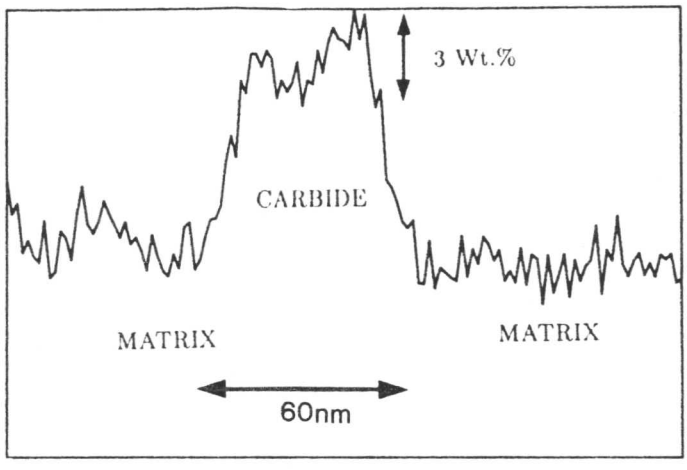

Figure 8.12: The concentration profile of chromium across a carbide and into the surrounding matrix measured using energy–dispersive X–ray analysis in a STEM from a specimen which has been tempered for 178 hours at 565°C.

8.4 Conclusions

The most important result is that, consistent with theoretical predictions the concentration of cementite at the cementite/ferrite interface is found to be far below that expected from equilibrium considerations. This is in samples which are annealed at elevated temperatures in order to permit the initially non–equilibrium cementite to enrich in chromium concentration. The apparent clusters of molybdenum and carbon atoms found in the ferrite matrix of specimens tempered for only 10 mins at 565°C using atom probe analysis, could indicate the early stages of Mo_2C formation, although much further work is needed to establish this quantitatively.

The diffusion coefficient of chromium in cementite needs to be established accurately, although this would be easier in a steel of slightly different composition in which the precipitates were more conducive to atom probe analysis.

STEM analyses have proved difficult for the magnetic specimens and the large interference from the predominantly iron containing matrix means that quantitative analyses are difficult, although used in conjunction with TEM on carbon extraction replicas they can provide useful information.

CHAPTER 9

FURTHER THEORETICAL STUDIES

In this chapter the question of whether simultaneous particle coarsening and enrichment can occur is addressed. It is shown quantitatively that the driving forces for the two processes are of opposite sign, and that the enrichment process appears to defeat coarsening until the bainitic carbides have reached their equilibrium compositions.

CHAPTER 9

FURTHER THEORETICAL STUDIES

9.1 Introduction

Particle coarsening is the dissolution of small precipitates and the simultaneous growth of larger particles at a fixed volume fraction. Ultimately a system will tend towards only one large particle. The driving force for the process is a decrease in the total interfacial energy. Factors which need to be considered in the development of a full theory of particle coarsening include the size and shape of the particles, the relationship between size and solubility, and whether the reaction is diffusion or interface controlled. A distribution of particle sizes within a matrix causes concentration gradients, and therefore, in order for these to be maintained, atoms have to transfer across the interface between the particle and the matrix. If diffusion of atoms within the matrix is the rate–controlling step then the growth is said to be *diffusion controlled*, whereas if it is more difficult for an atom to cross the interface into the matrix, then growth is said to be *interface controlled.*

Theoretical growth rate equations for individual particles for both diffusion and interface controlled reactions have been derived by Greenwood (1956) and (1969), and then these have been incorporated into analyses of the dispersion as a whole by Wagner (1961) and Lifshitz and Slyozov (1961). A brief review of experimental studies of particle coarsening is presented in the next section. The equations governing the coarsening process are then discussed in detail together with the necesssary modifications to allow for the coarsening of particles in a solid matrix. The application of the theory to simultaneous particle coarsening and enrichment is then outlined.

9.2 Experimental studies of particle coarsening

Early experiments were performed under the conditions for which the Wagner, Lifshitz and Slyozov theories were developed, i.e. virtually pure particles in a liquid. This work has been reviewed by Greenwood (1969). Recent interest has, however, concentrated on extending the theory to account for precipitates in a solid matrix. In most cases, this has been studied successfully using thin foils and extraction replicas in a transmission electron microscope. The main area of interest in this work is the coarsening of carbide particles in steels, and so the previous work on the Fe–C system only will be reviewed here, although it shoud be noted that there have been considerable advances in studies on the Ni–Al system by Ardell (1969).

There have been many theories proposed in the literature for the mechanism of cementite coarsening. Hyam and Nutting (1956) measured the carbide particle size distribution during the tempering of four plain carbon steels in the temperature range 500–700°C. They then related the changes in the particle diameters on tempering to hardness measurements, from which they calculated the activation energy for the softening process, following the assumption that particle size and separation are directly responsible for changes in hardness. The value which they obtained led them to conclude that cementite coarsening is controlled by the self–diffusion of iron, rather than the diffusion of carbon. Mukherjee *et al.* (1969) have pointed out that these measurements are unreliable because changes in the matrix structure during tempering are not taken into consideration.

Oriani (1964) then considered that both the diffusion of carbon and the diffusion of iron should be taken into account. His argument was that the growth of a cementite precipitate requires a change in volume according to the equation

$$Fe_3C \rightleftharpoons 3Fe + C\,,$$

which must be accommodated at both the growing and dissolving precipitates which necessitates coupled diffusion of iron and carbon. There was limited agreement of this theory with the experimental data due to approximations having to be made for the values of various constants.

Oriani's theory of coupled diffusion was then challenged by Björkland *et al.* (1972) who studied the effect of alloying elements on the rate of Ostwald ripening of cementite. They used a sophisticated treatment of the thermodynamics of the problem, but a rather basic treatment of the diffusion. They suggested that the diffusion coefficient may be reduced by elements dissolved in the cementite which diffuse very slowly and are therefore rate–controlling. They predicted that a Mn content of 0.001 wt.% in an Fe–C alloy would decrease the growth rate by a factor of 10. This idea is supported by Mukherjee *et al.* (1969), who studied the effect of chromium on carbide coarsening. They found that increasing the chromium content retarded the growth of cementite particles, and that the coarsening rate of the various chromium–based alloy carbides decreased in the order $Fe_3C, M_3C, M_{23}C_6, M_7C_3$. It is interesting to note that they found that M_3C and M_7C_3 coarsened at a rate consistent with the diffusion of chromium being rate–controlling, whereas the coarsening of Fe_3C is too rapid for the equivalent diffusion of iron to be rate–controlling.

An alternative interface controlled coarsening mechanism was proposed by Heckel and De Gregorio (1965). They studied a spheroidised eutectoid steel containing 0.75 wt.% C, and with other elements, such as Si and Ni, being present at levels of less than 0.005 wt.%. They

concluded that interface controlled kinetics were applicable having obtained coarsening rates two or three times lower than those predicted by carbon diffusion being rate–controlling. One possible explanation, however, is that even the small amounts of impurities present are retarding the coarsening. Heckel and De Gregorio proposed that the coarsening rate is limited by the rate of formation of cementite at the growing interfaces where the interfacial reaction is proportional to the solute thermodynamic activity gradient across the interface.

Another important factor considered by Mukherjee *et al.* (1969) is the influence of the matrix structure on coarsening rates. They found that the fine grain size and dislocation substructure in a martensitic microstructure caused a significant increase in the coarsening rate. They also noted that irregularities in particle size distribution curves could be resolved by the superposition of two different distributions, one from particles within the matrix and one from particles situated on the grain boundaries, caused by a transfer of material from the matrix to grain boundaries during tempering.

9.3 Particle size and solubility

The starting point for a theory of coarsening must be to relate the size of a particle to its solubility. The simplest relationship is the Gibbs–Thomson or Thomson–Freundlich equation for spherical particles of radius r, with an interfacial energy per unit area γ. The complete theory is given in Christian (1975) from which the following synopsis is taken.

Consider an assembly in which θ (cementite) particles of surface area O and surface free energy per unit area γ are in equilibrium with the α (ferrite) matrix. It can be shown that the energy of the interfaces displaces the equilibrium condition, and may be considered to contribute an additional thermodynamic potential, resulting in the fact that the solubility limit, $c^{\alpha\theta}$, and the equilibrium composition, $c^{\theta\alpha}$, of the cementite may both vary with the radius of the particle. The quantities relating to interface curvature are denoted by c_r^α and c_r^θ, where r is the particle radius, and those referring to the equilibrium compositions for infinite planar interfaces by c_∞^α and c_∞^θ. (N.B. Concentrations are used here rather than atomic fractions which are valid only when there is a negligible volume change on transformation. However, this assumption is implicit here because no strain energy terms due to the transformation are included in the treatment.)

The effect can be illustrated as follows. If a virtual change is considered in which dn atoms are transferred from the α phase to the θ phase, there will be an increase in the surface area of the θ particles, and therefore a corresponding increase in energy of γdO. This may be

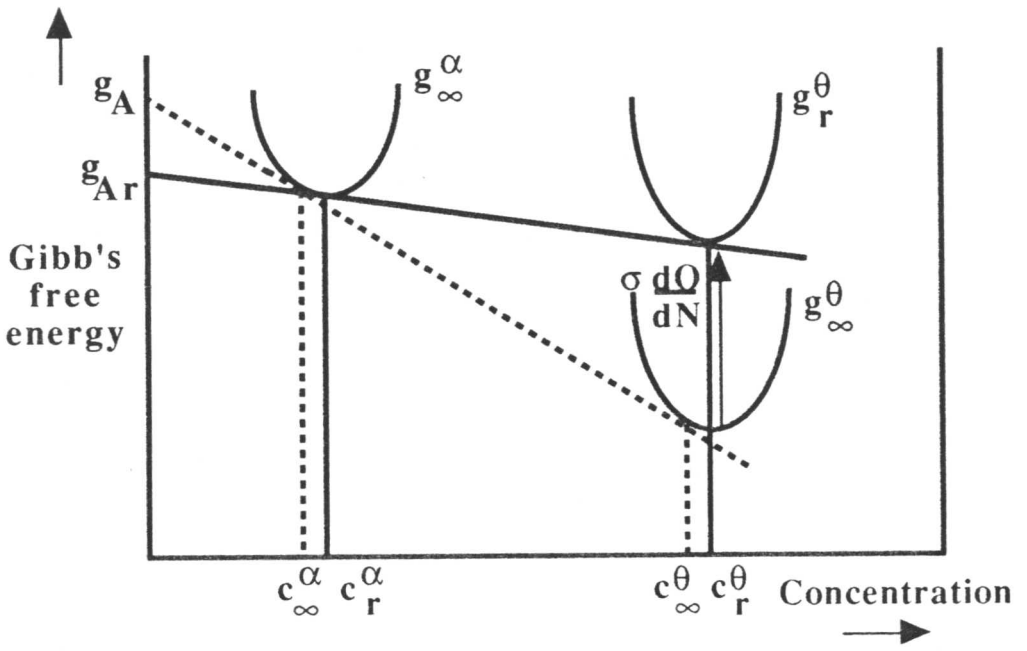

Figure 9.1: Free energy curves versus composition to illustrate the Gibbs–Thomson effect, (based on Christian, 1975).

represented as a displacement of the free energy per atom from g^{θ} to g^{θ}_{r} where

$$g^{\theta}_{r} = g^{\theta} + \gamma \frac{dO}{dn} \ . \tag{9.1}$$

The new equilibrium compositions are given by the common tangent construction to the free energy curves, as illustrated in Figure 9.1.

The effective chemical potentials per atom for curved interfaces are denoted by g^{θ}_{Ar} and g^{θ}_{Br}, and the new equilibrium conditions are $g^{\theta}_{Ar} = g^{\alpha}_{Ar}$ and $g^{\theta}_{Br} = g^{\alpha}_{Br}$. From the geometry of the diagram, it can be seen that

$$\Delta c^{\alpha}_{r} = c^{\alpha}_{r} - c^{\alpha}_{\infty} \tag{9.2}$$

which is of the same order of magnitude as

$$\Delta c^{\theta}_{r} = c^{\theta}_{r} - c^{\theta}_{\infty} \ , \tag{9.3}$$

and also that the approximation,

$$g^{\alpha}_{Br} - g^{\alpha}_{B\infty} = \frac{1 - c^{\alpha}_{\infty}}{c^{\theta}_{\infty} - c^{\alpha}_{\infty}} \gamma \frac{dO}{dn} \ , \tag{9.4}$$

can be made. The chemical potentials per atom of an ideal solution can be expressed as

$$g_A - g^0_A = kT \ln (1 - x) \text{ and} \tag{9.5}$$

$$g_B - g^0_B = kT \ln x \ , \tag{9.6}$$

where g^0 refers to the chemical potential of the pure substance. The absolute activity, λ, is defined in terms of the chemical potential as

$$g_A = kT \ln \lambda_A \ . \tag{9.7}$$

Equations 9.5 and 9.6 can then be written in terms of absolute activities as

$$\frac{\lambda_A}{\lambda_A^0} = \ln (1 - x) \text{ and} \tag{9.8}$$

$$\frac{\lambda_B}{\lambda_B^0} = \ln x \ , \tag{9.9}$$

where λ^0 refers again to the pure substance. Equations 9.8 and 9.9 can then be modified to take into account non–ideal solutions by multiplying their right hand sides by the appropriate experimentally measured activity coefficients, such that

$$\frac{\lambda_A}{\lambda_A^0} = \Gamma_A \ln (1 - x) \text{ and} \tag{9.10}$$

$$\frac{\lambda_B}{\lambda_B^0} = \Gamma_B \ln x \ . \tag{9.11}$$

Therefore, by substitution of the activity coefficients, Γ^α_{Br} and $\Gamma^\alpha_{B\infty}$, it can be shown that

$$g^\alpha_{Br} - g^\alpha_{B\infty} = kT \ln \left(\frac{\Gamma^\alpha_{Br} c_r^\infty}{\Gamma^\alpha_{B\infty} c^\alpha_\infty} \right), \tag{9.12}$$

and then, using the dilute solution approximation that Γ^α_B=constant and equating equations 9.4 and 9.12 gives

$$\frac{\Delta c_r^\alpha}{c^\alpha_\infty} \simeq \ln \left(\frac{c_r^\alpha}{c^\alpha_\infty} \right) = \frac{\gamma}{kT} \left(\frac{dO}{dn} \right) \left(\frac{1 - c^\alpha_\infty}{c^\theta_\infty - c^\alpha_\infty} \right) \ . \tag{9.13}$$

Using the approximation that the particles are spherical, for which

$$O = 4\pi r^2 \ \text{ and } \ n = \frac{4\pi r^3}{3V_m}, \tag{9.14}$$

where V_m is the molar volume and n is the number of atoms per mole, and then using the properties of partial derivatives,

$$\frac{\partial O}{\partial n} = \frac{\partial O}{\partial r} . \frac{\partial r}{\partial n} = \frac{2V_m}{r} \ , \tag{9.15}$$

equation 9.13 is simplified to the form usually used as the basis of coarsening theory,

$$\ln \left(\frac{c_r^\alpha}{c^\alpha_\infty} \right) = \frac{2\gamma V_m}{kTr} \left(\frac{1 - c^\alpha_\infty}{c^\theta_\infty - c^\alpha_\infty} \right) \ , \tag{9.16}$$

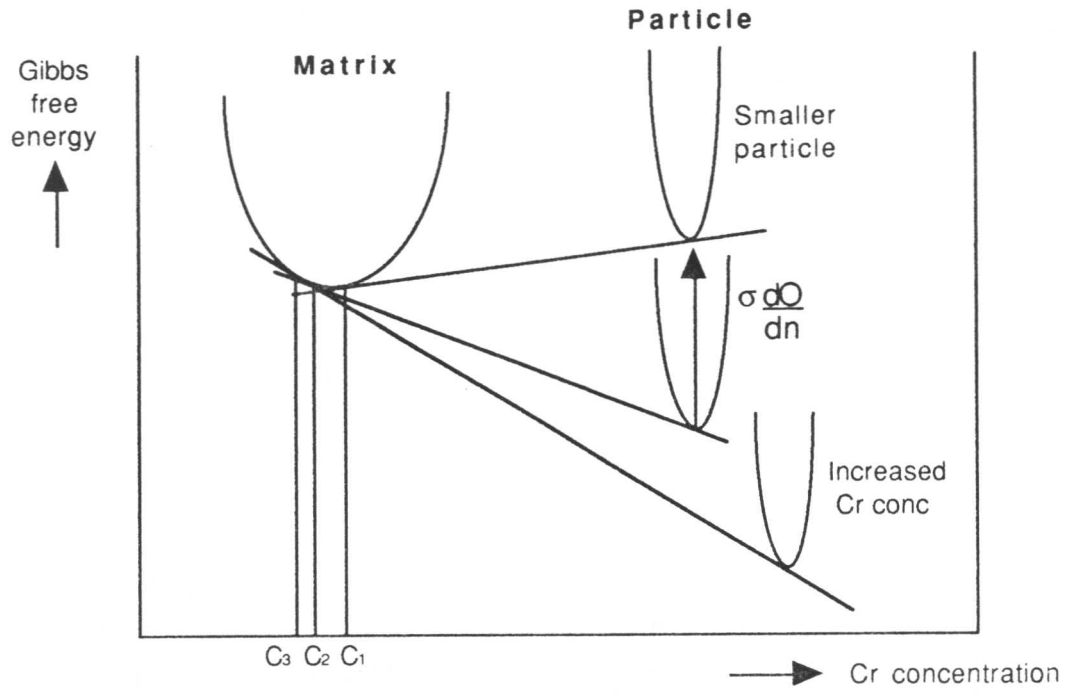

Figure 9.2: Schematic illustration of the increase in free energy due to particle curvature and the decrease in free energy due to increased thermodynamic stability.

equilibrium level, and that there is a constant volume fraction of precipitate. Oriani (1964) also points out that Wagner (1961) assumes that the atoms in the matrix offer no resistance to the motion of an interface, i.e. that the matrix atoms move at a much greater rate than the diffusion of the solute, and can therefore be neglected.

9.5 Application to simultaneous coarsening and enrichment of cementite

In order to address the question of whether or not particle coarsening (in the strictest sense) can occur whilst the process of enrichment is occurring the driving forces for the two reactions need to be investigated. It has been shown in the previous section that the driving force for coarsening originates from an increase in free energy due to particle curvature of a smaller particle. However, diffusion of chromium, for example, to cementite particles is driven by a reduction in free energy as thermodynamic equilibrium is approached. The driving forces for enrichment and coarsening will therefore tend to oppose each other. It has also been shown that smaller particles will enrich more quickly than larger particles and therefore the reduction in free energy due to an increased chromium content will be most marked for the smaller particles, thus cancelling out, to a certain extent, any increase in free energy due to an increased radius of curvature. This is illustrated schematically in Figure 9.2. These two opposing processes are quantified in the following sections.

9.5.1 Increase in free energy due to particle curvature

The increase in concentration of solute in the matrix surrounding a small particle has been discussed in section 9.3. An alternative approach is to consider the increase in free energy due to interface curvature. The expression for the increase in free energy due to interface curvature is given by the expression

$$\gamma \frac{\partial O}{\partial n} = \frac{2V_m\gamma}{r} \ . \tag{9.20}$$

For cementite, a value of γ given by Puls and Kirkaldy (1972) is 0.6 Jm^{-2}. The molar volume can be estimated from the unit cell dimensions and the number of atoms contain in one unit cell: cementite is orthorhombic with lattice parameters a=4.523Å, b=5.089Å and c=6.743Å, and there are 12 atoms contained in one unit cell. V_m is therefore given by

$$V_m = \frac{(4.523 \times 5.089 \times 6.743 \times 10^{-30})}{12} \times N_A \ , \tag{9.21}$$

where N_A is Avagadro's number. The increases in free energy for particle sizes of 10, 100 and 10000 nm are presented in Table 9.1. As expected the largest increase corresponds to the smallest particle size.

Table 9.1: Increase in free energy as a function of particle size.

Particle size /nm	Inc. in free energy /J mol^{-1}
10	934
100	93.4
10000	0.934

9.5.2 Decrease in free energy due to increased thermodynamic stability

In order to quantify the decrease in free energy due to an increase in thermodynamic stability because of an increase in chromium content of the cementite, an expression for the free energy of cementite is required. Lundberg *et al.* (1977) state that the molar Gibbs free energy os cementite is given by

$$G_m = y_{Fe}G^o_{FeC_{\frac{1}{3}}} + y_{Cr}G^o_{CrC_{\frac{1}{3}}} + RT(y_{Fe}\ln y_{Fe} + y_{Cr}\ln y_{Cr}) + y_{Fe}y_{Cr}A_o \ , \tag{9.22}$$

where y_{Fe} and y_{Cr} are concentration parameters related to the ordinary mole fractions, x, by

$$y_{Cr} = 1 - y_{Fe} = \frac{x_{Cr}}{1 - x_C} \ . \tag{9.23}$$

Other data are $G^o_{FeC_{\frac{1}{3}}}$=74,113 J mol^{-1}, $G^o_{CrC_{\frac{1}{3}}}$=-13,578 J mol^{-1} and A_o=1,790 J mol^{-1}. Cementite is virtually stoichiometric with respect to carbon content and therefore it contains 0.0067 mole fraction carbon. Evaluating this expression for particles containing various proportions of chromium and iron indicates that addition of 1 at.% Cr lowers the free energy of the cementite by approximately 1 kJ mol^{-1}.

These results are summarised in Figure 9.3. It has been shown in previous chapters that chromium concentration varies linearly with reciprocal particle size. Calculations were performed using the finite difference model to determine the chromium concentration as a function of tempering time for typical sizes and concentrations of the cementite particles found in the $2\frac{1}{4}$Cr1Mo steel. The predicted value of chromium concentration was then converted into a value of Gibbs free energy (using equation 9.22). An additional contribution to the free energy due to the capillarity effect was then added to give the total free energy. It can be seen from the plots of total free energy as a function of reciprocal size in Figure 9.3, for three different tempering times, that smaller particles become increasingly more stable than the larger ones. The contribution to the free energy from the capillarity term is also plotted for comparison. It is clear that capillarity is a very small effect compared with the fact that the larger particles enrich more slowly than the smaller ones.

9.6 Conclusions

The above results suggest that coarsening is defeated by the fact that in a distribution of particle sizes, the smaller particles will be richer in chromium and will not be able to give up chromium to the larger particles, as is the case in a true coarsening reaction, due to the opposite driving forces for the two reactions. Coarsening, in the true sense, will not therefore become important until the very late stages of ageing.

This argument explains why coarsening is not observed for the bainitic cementite discussed in Chapter 5. It has already been shown in Chapter 6 that pearlitic cementite particles are much larger than bainitic cementite and therefore the sensitivity to particle size effects is much reduced. However, for pearlitic cementite the lamellae are observed to spheroidise during the enrichment process (Figure 6.1). This can be thought of as a shape change from the initally coarse plate–shaped lamellae, rather than coarsening itself. In the absence of enrichment with respect to substitutional alloying elements, the spheroidisation rate would presumably be much faster.

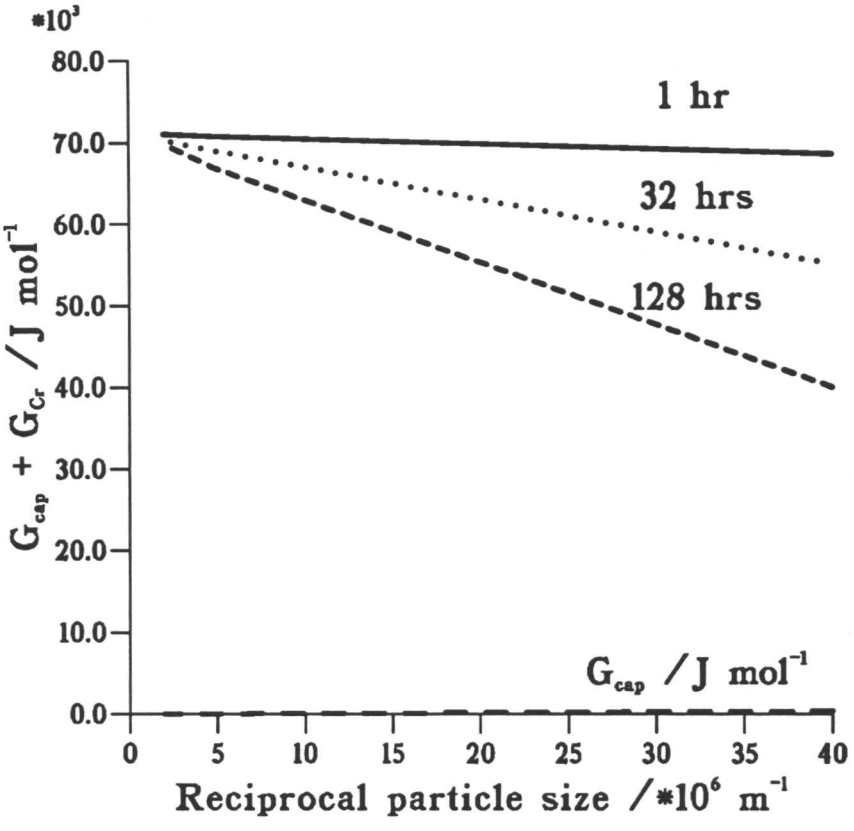

Figure 9.3: Total Gibbs free energy as a function of particle size after different enrichment times for cementite particles in $2\frac{1}{4}$Cr1Mo steel.

CHAPTER 10

CONCLUSIONS AND SUGGESTIONS FOR FUTURE WORK

CHAPTER 10

CONCLUSIONS AND SUGGESTIONS FOR FUTURE WORK

It is now possible to interpret fundamentally carbide enrichment kinetics of the kind associated with remanent life prediction in power plant steels. Thus it is, in principle, possible to extrapolate carbide chemistries with confidence over the sort of time scales typical of elevated temperature applications. Specifically, the precipitation characteristics of three power plant steels containing different chromium concentrations, $\frac{1}{2}$Cr$\frac{1}{2}$Mo$\frac{1}{4}$V, 2$\frac{1}{4}$Cr1Mo and 12Cr1MoV, have been studied in detail.

$\frac{1}{2}$Cr$\frac{1}{2}$Mo$\frac{1}{4}$V steel, being pearlitic, was found to contain relatively large cementite particles. As a consequence of this, the substitutional alloy content of the cementite is not particularly sensitive to particle size. The low chromium content in the steel means that the equilibrium concentration of chromium in the cementite is low. This results in a much smaller degree of enrichment during ageing, thereby reducing the sensitivity to the particle size. The agreement between the theoretical model and the experimentally measured enrichment data is found to be very good. For this steel, measurement of cementite composition change can prove a valuable indicator of the average thermal history, and therefore of the remanent creep life.

Power plant components are very large, and therefore the microstructure can vary considerably through the section of a given component. Studies of the precipitation characteristics in the 2$\frac{1}{4}$Cr1Mo steel have highlighted the importance of cementite composition being related to the position in the microstructure. Significantly different enrichment rates have been observed in fully bainitic and mixed ferritic/bainitic microstructures. The much larger equilibrium concentration of chromium in cementite and the smaller size of bainitic carbides in this steel result in the measured chromium concentration being very sensitive to particle size, the smaller particles enriching more quickly than the larger ones. It has also been shown that when alloy carbides co–exist in the microstructure with cementite, the cementite composition no longer changes in a simple manner. The precipitation of chromium–rich alloy carbides can substantially reduce the chromium level in the cementite.

The kinetics of precipitation have been found to be extremely rapid in the 12Cr1MoV steel. The equilibrium alloy carbide precipitates during the stress–relief heat treatment and subsequently does not change in composition. It is perhaps not surprising that changes in alloy carbide chemistries, induced by tempering, are found to be less striking than those observed for cementite. The growth of alloy carbides involves considerable long range diffusion and there is therefore greater opportunity for the carbide to be closer to equilibrium when it first forms.

The derivation of this approximation is given below. The Taylor expansions on the $(j+1)^{th}$ time row are:-

$$c_{i+1,j+1} = c_{i,j+1} + \delta r \left(\frac{\partial c}{\partial r}\right)_{i,j+1} + \frac{1}{2}(\delta r)^2 \left(\frac{\partial^2 c}{\partial r^2}\right)_{i,j+1} + \ldots \tag{I.7}$$

$$c_{i-1,j+1} = c_{i,j+1} - \delta r \left(\frac{\partial c}{\partial r}\right)_{i,j+1} + \frac{1}{2}(\delta r)^2 \left(\frac{\partial^2 c}{\partial r^2}\right)_{i,j+1} + \ldots . \tag{I.8}$$

Subtraction and addition of these two equations lead respectively to the following equations:-

$$\left(\frac{\partial c}{\partial r}\right)_{i,j+1} = \frac{c_{i+1,j+1} - c_{i-1,j+1}}{2\delta r} \tag{I.9}$$

$$\left(\frac{\partial^2 c}{\partial r^2}\right)_{i,j+1} = \frac{c_{i+1,j+1} - 2c_{i,j+1} + c_{i-1,j+1}}{\delta r^2} . \tag{I.10}$$

Then, using the approximation that

$$\left(\frac{\partial c}{\partial r}\right) = \frac{1}{2}\left[\left(\frac{\partial c}{\partial r}\right)_{i,j+1} + \left(\frac{\partial c}{\partial r}\right)_{i,j}\right] , \tag{I.11}$$

$$\left(\frac{\partial^2 c}{\partial r^2}\right) = \frac{1}{2}\left[\left(\frac{\partial^2 c}{\partial r^2}\right)_{i,j+1} + \left(\frac{\partial^2 c}{\partial r^2}\right)_{i,j}\right] , \tag{I.12}$$

the following expressions can be obtained:-

$$\left(\frac{\partial c}{\partial r}\right) = \frac{1}{2}\left[\frac{c_{i+1,j+1} - c_{i-1,j+1}}{2(\delta r)} + \frac{c_{i+1,j} - c_{i-1,j}}{2(\delta r)}\right] , \text{ and} \tag{I.13}$$

$$\left(\frac{\partial^2 c}{\partial r^2}\right) = \frac{1}{2}\left[\frac{c_{i+1,j+1} - 2c_{i,j+1} + c_{i-1,j+1}}{(\delta r)^2} + \frac{c_{i+1,j} - 2c_{i,j} + c_{i-1,j}}{(\delta r)^2}\right] . \tag{I.14}$$

This is termed the *implicit* finite difference method because unknowns on the time level $(j+1)$ are expressed in terms of known values on the time level j. Therefore, N grid points result in N simultaneous equations to solve in order to obtain the unknown values. More computation is required at each step than with the explicit finite difference method, but this calculation remains stable for all values of δt, whereas the explicit method is only stable for $\delta t \leq 0.5\delta r^2$ and therefore it is possible to use larger and therefore fewer time steps.

APPENDIX II

FINITE.FOR

```
C Program using finite difference method for the solution of the problem
C of X enrichment of cementite during the ageing of bainitic steels
C
C EQFER = Equilibrium at.% of X in ferrite at ageing temperature
C EQCEM = Equilibrium at.% of X in cementite at ageing temperature
C EBAR = Average X at.% in alloy
C FERS = normalised concentration of X at ferrite surface
C CEMS = normalised concentration of X at cementite surface
C TIMH = time in hours
C KTEMP = Absolute temperature
C TCEM = Thickness of cementite in meters
C TFER = Half-thickness of ferrite in meters
C N.B. This is calculated from the volume fraction of chromium
C in the alloy in the program
C
C DFER = Diffusivity of X in ferrite
C DCEM = Diffusivity of X in cementite
C Q = Activation free energy for diffusion
C FREQ = Pre-exponential factor for diffusion
C The mean size of a cementite particle is usually taken to be 100nm
C (This is based on experimental experience)
C
C Concentrations normalized relative to average alloy concentration
C Dimension normalize relative to carbide particle thickness
C ICEM, IFER, J1 are the number of finite slices
C for dimension and time respectively
C (N.B. ICEM is read into this program but IFER is calculated: both
C values must be transferred to FINN via the dataset)
C TIM = Time, in seconds
C A3 controls the amount of information that is printed out
C SETIME controls the time in hours that the experiment runs.
C JTEST modifies the mass balance condition when the CEMS reaches
C the equilibrium concentration. Hence mass is conserved.
C
C Typical data
C 838.15 0.5D-03 39.0D+00 2.5D+00 1.0D-07 0.1 5
C 0.0003D+00 2.0D+00 1.0 1.0
C 2.53D-04 240580.0 (DIFFUSION DATA, JOULES ETC.)
C End of data
C
      IMPLICIT REAL*8(A-H,K-Z), INTEGER(I,J)
      DOUBLE PRECISION CFER(1500,2), CCEM(20,2)
      J4 = 0
      J5 = 0
      JTEST = 0
      READ(5,*) KTEMP,EQFER,EQCEM,EBAR,TCEM,VOLUME,ICEM
```

```
      READ(5,*) CFER(1,1),CCEM(1,1),A3,SETIME
      READ(5,*) FREQ,Q
      RFER = 0.40D+00
      RCEM = RFER
      TFER = (TCEM*(1.0D+00-VOLUME))/(2*VOLUME)
      DFER = DIFF(KTEMP,Q,FREQ)
      DCEM = DIFF(KTEMP,Q,FREQ)
      STCEM = 0.5D+00*TCEM/ICEM
      IFER = DINT(TFER/STCEM)
      STFER = TFER/IFER
      TIME = RFER*STFER*STFER/DFER
      J1 = DINT(3600*SETIME/TIME)
      WRITE(6,100) DFER,DCEM,VOLUME,TFER,TCEM,EQFER,EQCEM,KTEMP,ICEM
     + ,IFER,STCEM,STFER
      DO  1 I = 2,ICEM
          CCEM(I,1) = 1.0D+00
1     CONTINUE
      DO  2 I = 2,IFER
          CFER(I,1) = 1.0D+00
2     CONTINUE
C
      FERS = EQFER/EBAR
      DR = DFER/DCEM
      WRITE(6,101) CCEM(1,1),CFER(1,1)
C
C Finite difference analysis
C
      TIM = 0.0D+00
      WRITE(6,102)
      DO  50 J = 2,J1
          TIM = TIM+TIME
          TIMH = TIM/3600.0D+00
          IF (TIMH .GT. SETIME) GOTO 51
              CEMM = 0.0D+00
              FERR = 0.0D+00
C
C               ****** Ferrite ******
C
              DO  10 II = 1,IFER
                  IF (II .EQ. 1) THEN
C Note: surface concentration in ferrite is at equilibrium
C until CEMS reaches the equilibrium concentration
                      IF (JTEST .EQ. 0) THEN
                          CFER(1,2) = CFER(1,1) + RFER*(FERS - 2.0D+00*CFER(1,1)
     +                    + CFER(2,1))
                      ELSE
                          FERS = ((CCEM(1,1)-CEMS)/DR) + CFER(1,1)
                      ENDIF
C Ensure reflection at last slice
                  ELSEIF (II .EQ. IFER) THEN
                      CFER(IFER,2) = CFER(IFER,1)+RFER*(CFER(IFER-1,1)
```

```
     +                  -2.0D+00*CFER(IFER,1)+CFER(IFER-1,1))
                        CALL SOFT(CFER(IFER,2),1,J4,TIMH)
                      ELSE
                        CFER(II,2) = CFER(II,1)+RFER*(CFER(II-1,1)
     +                  -2.0D+00*CFER(II,1)+CFER(II+1,1))
                      ENDIF
                      FER = CFER(II,2)*EBAR
                      XTFER = STFER*II
                      FERR = FER+FERR
                      CFER(II,1) = CFER(II,2)
10                  CONTINUE
C
C                 ******** Cementite ********
C
                    DO  20 I = 1,ICEM
C Calculate surface concentration in cementite
C appropriate for mass balance
                      IF (I .EQ. 1) THEN
                        CEMS = DR*(CFER(1,1)-FERS)+CCEM(1,1)
C Reflect at position of symmetry
                        IF (CEMS .GT. (EQCEM/EBAR)) THEN
                          CEMS = EQCEM/EBAR
                          JTEST = 1
                        ELSE
                          CCEM(1,2) = CCEM(1,1) + RCEM*(CEMS-2.0D+00*CCEM(1,1)
     +                    + CCEM(2,1))
                        ENDIF
                      ELSEIF (I .EQ. ICEM) THEN
                        CCEM(ICEM,2) = CCEM(ICEM,1)+RCEM*(CCEM(ICEM-1,1)
     +                  -2.0D+00*CCEM(ICEM,1)+CCEM(ICEM-1,1))
                        CALL SOFT (CCEM(ICEM,2),2,J5,TIMH)
                      ELSE
                        CCEM(I,2) = CCEM(I,1)+RCEM*(CCEM(I-1,1)
     +                  -2.0D+00*CCEM(I,1)+CCEM(I+1,1))
                      ENDIF
                      CEM = CCEM(I,2)*EBAR
                      XTCEM = I*STCEM
                      CEMM = CEM+CEMM
                      CCEM(I,1)=CCEM(I,2)
20                  CONTINUE
C
                    CEMM = CEMM/ICEM
                    FERR = FERR/IFER
                    DUMMY = J/A3
                    DUMMY = DINT(DUMMY)-DUMMY
                    IF (DUMMY .EQ. 0.0) THEN
                      AVER = (FERR*TFER + CEMM*0.5D+00*TCEM)/(TFER+0.5D+00*TC
                      WRITE(6,103) TIMH,CEMM,FERR,AVER,FERS*EBAR,CEMS*EBAR
                    ENDIF
50                CONTINUE
51                WRITE(6,104)
```

```
                DO  60 I = 1,ICEM
                    IF (CCEM(I,2) .LT. 1.0001) GOTO 61
                        WRITE(6,105) I,CCEM(I,2),CCEM(I,2)*EBAR
60                  CONTINUE
61                  WRITE(6,106)
                    DO  70 J = 1,IFER
                        IF (CFER(J,2) .GT. 0.999) GOTO 71
                            WRITE(6,105) J,CFER(J,2),CFER(J,2)*EBAR
70                      CONTINUE
71                  CONTINUE
C
100                 FORMAT(' Diffusion coefficient in ferrite, m**2/s = ',
     +              D12.4/' Diffusion coefficient in cementite, m**2/s, = ',D12.4/
     +              ' Volume fraction of cementite (MTDATA) = ',D12.4/
     +              ' Half thickness of ferrite, m =',D12.4/
     +              ' Thickness of cementite, m =',D12.4/
     +              ' Eq. conc. of X at interface, in ferrite, at.% = ',D12.4/
     +              ' Eq. conc. of X at interface, in cementite, at.% = ',D12.4/
     +              ' Absolute Temperature = ', F8.2, ' ICEM, IFER = ',2I9/
     +              ' STCEM (m) = ',D12.4, ' STFER (m) = ',D12.4//)
101                 FORMAT(' Time 0, slice 1, cementite and ferrite norm conc ',
     +              2F12.4/)
102                 FORMAT(' HOURS CEM FERRITE AVERAGE X FERS CEMS')
103                 FORMAT(D10.2,F9.4, F9.4,F9.4,F9.4,2F9.4)
104                 FORMAT(' No Norm. Conc. at.%X in Cementite')
105                 FORMAT(I8,D12.4,2F10.4)
106                 FORMAT(' No Norm. Conc. at.%X in Ferrite')
                    STOP
                    END
. . . . . .
                    DOUBLE PRECISION FUNCTION DIFF(KTEMP,Q,FREQ)
                    DOUBLE PRECISION KTEMP, R, Q, FREQ
                    R = 8.3143
                    DIFF = FREQ*DEXP(-Q/(R*KTEMP))
C R = Universal Gas Constant, J/mol/K
C KTEMP = Absolute Temperature
C Data for X inter diffusion in alpha iron, from Fridberg (1969) paper
                    RETURN
                    END
. . . . . .
        SUBROUTINE SOFT (A,I,J,TIMH)
        DOUBLE PRECISION A,TIMH
        IF (J .GT. 1) RETURN
            IF (I .NE. 1) THEN
                IF (A .GT. 1.01D+00) THEN
                    WRITE(6,11) TIMH
                    J = 3
                ENDIF
            ELSEIF (A .LT. 0.99) THEN
                WRITE(6,10) TIMH
                J = 3
```

```
      ELSE
          RETURN
      ENDIF
      RETURN
10    FORMAT(' SOFT IMPINGEMENT IN FERRITE', F11.5,' hours')
11    FORMAT(' SOFT IMPINGEMENT IN CEMENTITE',F11.5,' hours')
      END
```

APPENDIX III

INHOMOG.FOR

```
C Program using finite difference method for the solution of the problem
C of X enrichment of cementite during the ageing of bainitic steels
C for an inhomogeneous carbon distribution.
C
C TIMH time in hours
C KTEMP=Absolute temperature
C TCEM=Thickness of cementite in meters
C EQFER=Equilibrium wt.% of X in ferrite at ageing temperature
C EQCEM=Equilibrium wt.% of X in cementite at ageing temperature
C EBAR=Average X wt.% in alloy
C DFER=Diffusivity of X in ferrite
C DCEM=Diffusivity of X in cementite
C Q = ACTIVATION FREE ENERGY FOR DIFFUSION
C FREQ = PRE-EXPONENTIAL FACTOR FOR DIFFUSION COEFFICIENT
C Concentrations normalized relative to average alloy concentration
C Dimension normalize relative to carbide particle thickness
C TIM = Time, in seconds
C A3 controls the amount of information that is printed out
C SETIME controls the time in hours that the experiment runs.
C JTEST modifies the mass balance condition when the CEMS reaches
C the equilibrium concentration. Hence mass conserved
C RATIO is the ratio of TFERA to TFERB (the relative sizes of the
C inhomogeneous ferrite distribution)
C
C
      IMPLICIT DOUBLE PRECISION(A-H,K-Z)
      INTEGER I,J
      DOUBLE PRECISION CFERA(1500,2), CFERB(1500,2), CCEM(1500,2)
      READ(5,*) KTEMP,EQFER,EQCEM,EBAR,TCEM,VOLFRAC,ICEM,RATIO
      READ(5,*) A3,SETIME,FREQ,Q
      J4=0
      J5=0
      J6=0
      JTESTA=0
      JTESTB=0
C Set up the initial conditions
      TFERB=(TCEM*(1-VOLFRAC))/(VOLFRAC*(1+RATIO))
      TFERA=TFERB*RATIO
      DFER=DIFF(KTEMP,Q,FREQ)
      DCEM=DIFF(KTEMP,Q,FREQ)
      RFER=0.4D+00
      RCEM=RFER
      DR=DFER/DCEM
      STCEM=TCEM/(ICEM+1)
      IFERA=DINT(TFERA/STCEM)
      IFERB=DINT(TFERB/STCEM)
```

```
            STFERA=TFERA/IFERA
            STFERB=TFERB/IFERB
C Set up time loop
            TIME=(RFER*STFERA*STFERA)/DFER
            J1=DINT(3600D+00*SETIME/TIME)
C Write out the initial program parameters
            WRITE(6,100) DFER,DCEM,VOLFRAC,TFERA,TFERB,TCEM,EQFER,EQCEM,
     +      KTEMP,ICEM,IFERA,IFERB,STCEM,STFERA,STFERB
C Set up the initial conditions everywhere
            DO  10 I=1,IFERA
                CFERA(I,1)=1.0D+00
10          CONTINUE
            DO  20 I=1,ICEM
                CCEM(I,1)=1.0D+00
20          CONTINUE
            DO  30 I=1,IFERB
                CFERB(I,1)=1.0D+00
30          CONTINUE
            IMID=INT(ICEM-1)/2
            FERSA=EQFER/EBAR
            FERSB=EQFER/EBAR
            TIM=0.0D+00
            DO  40 J=2,J1
                TIM=TIM+TIME
                TIMH=TIM/3600D+00
C For the calculation of the average composition in the phases
                CEMM=0.0D+00
                FERRA=0.0D+00
                FERRB=0.0D+00
C
C ************************FerriteA***************************
C
                DO  50 II=1,IFERA
                    IF (II .EQ. 1) THEN
                        IF (JTESTA .EQ. 0) THEN
                            CFERA(1,2)=CFERA(1,1)+RFER*
     +                      (FERSA-2.0D+00*CFERA(1,1)+CFERA(2,1))
                        ELSE
                            FERSA=((CCEM(1,1)-CEMSA)/DR)+CFERA(1,1)
                        ENDIF
                    ELSEIF (II .EQ. IFERA) THEN
                        CFERA(IFERA,2)=CFERA(IFERA,1)+RFER*(CFERA(IFERA-1,1)
     +                  -2.0D+00*CFERA(IFERA,1)+CFERA(IFERA-1,1))
                        CALL SOFT(CFERA(IFERA,2),1,J4,TIMH)
                    ELSE
                        CFERA(II,2)=CFERA(II,1)+RFER*(CFERA(II-1,1)
     +                  -2.0D+00*CFERA(II,1)+CFERA(II+1,1))
                    ENDIF
                    FERA=CFERA(II,2)*EBAR
                    XTFERA=STFERA*II
                    FERRA=FERA+FERRA
```

```
                    CFERA(II,1)=CFERA(II,2)
50                CONTINUE
C
C ************************FerriteB****************************
C
                  DO  60 II=1,IFERB
                      IF (II .EQ. 1) THEN
                          IF (JTESTB .EQ. 0) THEN
                              CFERB(1,2)=CFERB(1,1)+RFER*(FERSB-2.0D+00*CFERB(1,1
     +                        +CFERB(2,1))
                          ELSE
                              FERSB=((CCEM(1,1)-CEMSB)/DR)+CFERB(1,1)
                          ENDIF
                      ELSEIF (II .EQ. IFERB) THEN
                          CFERB(IFERB,2)=CFERB(IFERB,1)+RFER*(CFERB(IFERB-1,1)
     +                    -2.0D+00*CFERB(IFERB,1)+CFERB(IFERB-1,1))
                          CALL SOFT(CFERB(IFERB,2),2,J5,TIMH)
                      ELSE
                          CFERB(II,2)=CFERB(II,1)+RFER*(CFERB(II-1,1)
     +                    -2.0D+00*CFERB(II,1)+CFERB(II+1,1))
                      ENDIF
                      FERB=CFERB(II,2)*EBAR
                      XTFERB=STFERB*II
                      FERRB=FERB+FERRB
                      CFERB(II,1)=CFERB(II,2)
60                CONTINUE
C
C ************************Cementite***************************
C
                  DO  70 I=1,ICEM
C Calculate the surface concentration in cementite on border
C with ferrite A appropriate for mass balance
                      IF (I .EQ. 1) THEN
                          CEMSA=DR*(CFERA(1,1)-FERSA)+CCEM(1,1)
                          IF (CEMSA .GT. (EQCEM/EBAR)) THEN
                              CEMSA=EQCEM/EBAR
                              JTESTA=1
                          ELSE
                              CCEM(1,2)=CCEM(1,1)+RCEM*(CEMSA-2.0D+00*CCEM(1,1)
     +                        +CCEM(2,1))
                          ENDIF
                      ELSEIF (I .EQ. ICEM) THEN
C Calculate the surface concentration in cementite on border
C with ferrite B appropriate for mass balance
                          CEMSB=DR*(CFERB(1,1)-FERSB)+CCEM(ICEM,1)
                          IF (CEMSB .GT. (EQCEM/EBAR)) THEN
                              CEMSB=EQCEM/EBAR
                              JTESTB=1
                          ELSE
                              CCEM(ICEM,2)=CCEM(ICEM,1)+RCEM*(CCEM(ICEM-1,1)
     +                        -2.0D+00*CCEM(ICEM,1)+CEMSB)
```

```
                    ENDIF
                  ELSE
                    CCEM(I,2)=CCEM(I,1)+RCEM*(CCEM(I-1,1)-
     +              2.0D+00*CCEM(I,1)+CCEM(I+1,1))
                  ENDIF
                  IF (I .EQ. IMID) THEN
                    CALL SOFT(CCEM(IMID,2),3,J6,TIMH)
                  ENDIF
                  CEM=CCEM(I,2)*EBAR
                  XTCEM=I*STCEM
                  CEMM=CEM+CEMM
                  CCEM(I,1)=CCEM(I,2)
70              CONTINUE
C Write out the results
                CEMM=CEMM/ICEM
                FERRA=FERRA/IFERA
                FERRB=FERRB/IFERB
                DUMMY=J/A3
                DUMMY=DINT(DUMMY)-DUMMY
                IF (DUMMY .EQ. 0) THEN
                  AVER=(FERRA*TFERA+CEMM*TCEM+FERRB*TFERB)/
     +            (TFERA+TCEM+TFERB)
                  WRITE(6,101) TIMH, CEMM, FERRA, FERRB
     +            ,AVER, FERSA*EBAR, CEMSA*EBAR, CEMSB*EBAR, FERSB*EBAR
                ENDIF
40            CONTINUE
              WRITE(6,*) ' No wt.%X in FerriteA'
              DO  80 I = IFERA,1,-1
                WRITE(6,102) ((I-(IFERA+1))*-1)*STFERA,CFERA(I,2)*EBAR
80            CONTINUE
              WRITE(6,*) ' No wt.%X in Cementite'
              DO  90 I = 1,ICEM
                WRITE(6,102) (I+IFERA-1)*STCEM,CCEM(I,2)*EBAR
90            CONTINUE
              WRITE(6,*) ' No wt.%X in FerriteB'
              DO  95 I = 1,IFERB
                WRITE(6,102) (I+IFERA+ICEM-2)*STFERB,CFERB(I,2)*EBAR
95            CONTINUE
100           FORMAT(' Diffusion coefficient in ferrite, m**2/s = ',D12.4/
     +        ' Diffusion coefficient in cementite, m**2/s, = ',D12.4/
     +        ' Volume fraction of cementite (MTDATA) = ',D12.4/
     +        ' Thickness of ferriteA, m =',D12.4/
     +        ' Thickness of ferriteB, m =',D12.4/
     +        ' Thickness of cementite, m =',D12.4/
     +        ' Eq. conc. of X at interface, in ferrite, wt.% = ',D12.4/
     +        ' Eq. conc. of X at interface, in cementite, wt.% = ',D12.4/
     +        ' Absolute Temperature = ', F8.2/
     +        ' ICEM, IFERA, IFERB = ',3I9/
     +        ' STCEM (m) = ',D12.4/
     +        ' STFERA (m) = ',D12.4, ' STFERB (m) = ',D12.4//)
101           FORMAT(D10.4,3F8.3)
```

```
102             FORMAT(2D14.4)
                STOP
                END
. . . . . .
                DOUBLE PRECISION FUNCTION DIFF(KTEMP,Q,FREQ)
                DOUBLE PRECISION KTEMP, R, Q, FREQ
                R=8.3143
                DIFF=FREQ*DEXP(-Q/(R*KTEMP))
C R = Universal Gas Constant, J/mol/K
C KTEMP = Absolute Temperature
C Data for X tracer diffusion in alpha iron, from XC Handbook 57
                RETURN
                END
. . . . . .
        SUBROUTINE SOFT(A,I,J,TIMH)
        DOUBLE PRECISION A,TIMH
        IF (J .GT. 1) GOTO 99
            IF (I .EQ. 1) THEN
                IF (A .LT. 0.99D+00) THEN
                    WRITE(6,110) TIMH
                    J=3
                ENDIF
            ELSEIF (I .EQ. 2) THEN
                IF (A .LT. 0.99D+00) THEN
                    WRITE(6,111) TIMH
                    J=3
                ENDIF
            ELSEIF (I .EQ. 3) THEN
                IF (A .GT. 1.01D+00) THEN
                    WRITE(6,112) TIMH
                    J=3
                ENDIF
            ENDIF
110         FORMAT(' SOFT IMPINGEMENT IN FERRITEA', F11.5,' hours')
111         FORMAT(' SOFT IMPINGEMENT IN FERRITEB', F11.5,' hours')
112         FORMAT(' SOFT IMPINGEMENT IN CEMENTITE', F11.5,' hours')
99          RETURN
            END
```

REFERENCES

AARONSON, H. I., (1986)
'Bainite Reaction', Encyclopedia of Materials Science and Technology, Pergamon Press, Oxford. p. 263–266.

AFROUZ, A., COLLINS, M. J. and PILKINGTON, R., (1983)
'Microstructural Examination of 1Cr0.5Mo Steel during Creep', *Metals Technology,* **10,** p. 461–463.

ALBERRY, P. J. and GOOCH, D. J., (1983)
'12CrMoV-A status review', Central Electricity Generating Board Report TRPD/L/2506/N83.

AL-SALMAN, S. A., LORIMER, G. W. and RIDLEY, N., (1979)
'Pearlite Growth Kinetics and Partitioning in a Cr–Mn Eutectoid Steel', *Metallurgical Transactions A,* **10A,** p. 1703–1709.

ANDREWS, K. W. and HUGHES, H., (1958)
'Micro-constituents in Steels; Their Electrolytic Isolation and X-ray Study', *Iron and Steel,* **30,** p. 43–50.

ANDREWS, K. W., DYSON, D. J., and KEOWN, S. R., (1967)
'Interpretation of electron diffraction patterns', Publ. Hilger and Watts, London.

ANDREWS, K. W., HUGHES, H. and DYSON, D. J., (1972)
'Constitution diagrams for Cr–Mo–V steels', *Journal of the Iron and Steel Institute,* **191,** p. 337–350.

ARDELL, A. J., (1969)
'Experimental confirmation of the Lifshitz–Wagner theory of particle coarsening', in 'The mechanism of phase transformations in crystalline solids', *Institute of Metals Monograph No. 33,* p. 111–116.

ARGENT, B. B., VAN NIEKERK, M. N. and REDFERN, G. A., (1970)
'Creep of ferritic steels', *Journal of the Iron and Steel Institute,* **208,** p. 830–843.

AVRAMI, M., (1939)
'Kinetics of Phase Changes I', *Journal of Chemical Physics,* **7,** p. 1103.

BAKER, R. G. and NUTTING, J., (1959)
'The tempering of 2.25Cr1Mo Steel after Quenching and Normalizing', *Journal of the Iron and Steel Institute,* **191,** p. 257–268.

BARNARD, S. J., SMITH, G. D. W., GARRETT-REED, A. J. and VANDER SANDE, J., (1987)
'Atom Probe Studies (2) Low Temperature Chromium Diffusivity in Bainite', Proceedings of International Conference on Solid State Phase Transformations, Pittsburgh, USA.

BARRACLOUGH, D. R. and GOOCH, D. J., (1985)
'Effect of inadequate heat treatment on creep strength of 12CrMoV steel', *Materials Science and Technology,* **1,** p. 961–967.

BARRETT, C. S. and MASSALSKI, T. B., (1968)
'Structure of Metals and Alloys', McGraw-Hill, New York.

BATTAINI, P., D' ANGELO, D., MARINO, G. and HALD, J., (1990)
'Interparticle Distance Evolution on Steam Pipes of 12Cr1Mo1V Steel during Power Plant Service Times', in 'Proceedings of the 4th International Conference of the Creep and Fracture of Engineering Materials', Swansea, Eds. B. Wilshire and R. W. Evans.

BEECH, J. and WARRINGTON, D. H., (1966)
'M_7C_3 to $M_{23}C_6$ transformation in chromium containing alloys', *Journal of the Iron and Steel Institute,* **204,** p. 460–468.

BERRY, F. G. and HONEYCOMBE, R. W. K., (1970)
'The Isothermal Decomposition of Austenite in Fe–Mo–C alloys', *Metallurgical Transactions,* **1,** p. 3279–3286.

BHADESHIA, H. K. D. H., (1981)
'Bainite: The Incomplete–Reaction phenomenon and the approach to equilibrium', Proceedings of the International Solid–Solid Phase Transformation Conference, Pittsburgh. p. 1041–1048.

BHADESHIA, H. K. D. H., (1982)
'A Thermodynamic Analysis of Isothermal Transformation Diagrams', *Metal Science,* **16,** p. 159–165.

BHADESHIA, H. K. D. H., (1985)
'Diffusional Formation of Ferrite in Iron and its Alloys', *Progress in Materials Science, Pergamon Press, Oxford,* **29,** p. 321–386.

BHADESHIA, H. K. D. H., (1987)
'Worked Examples in the Geometry of Crystals', The Institute of Metals, London.

BHADESHIA, H. K. D. H., (1988)
'Bainite in Steels', Phase Transformations '87, Institute of Metals, London, ed. G. W. Lorimer, p. 309–314.

BHADESHIA, H. K. D. H., (1989)
'Theoretical Analysis of Changes in Cementite Composition During Tempering of Bainite', *Materials Science and Technology,* **5,** p. 131–137.

BHADESHIA, H. K. D. H., (1992)
'Bainite in Steels', The Institute of Materials, London.

BHADESHIA, H.K.D.B. and EDMONDS, D. V., (1979)
'The Bainite Transformation in a Silicon Steel', *Metallurgical Transactions A,* **10A,** p. 895–907.

BHADESHIA, H. K. D. H. and WAUGH, A. R., (1982)
'Bainite: An atom probe study of the Incomplete–Reaction phenomenon', *Acta Metallurgica,* **30,** p. 775–784.

BHADESHIA, H. K. D. H., SWENSSON, L.–E. and GRETOFT, B., (1987)
'Theory for allotriomorphic ferrite formation in steel weld deposits', Welding metallurgy of structural steels, ed. J. Y. Koo, TMS–AIME, Warrendale, Penn., USA. p. 517–530.

BHADESHIA, H. K. D. H. and CHRISTIAN, J. W., (1990)
'Bainite in Steels', *Metallurgical Transactions A,* **21A,** p. 767–797.

BJÄRBO, A., (1991)
Ph.D. Thesis, Royal Institute of Technology, Sweden.

BJÖRKLAND, S., DONAGHEY, L. F. and HILLERT, M., (1972)
'The effect of alloying elements on the rate of Ostwald ripening of cementite in steel', *Acta Metallurgica,* **20,** p.867–874.

BOWEN, A. W. and LEAK, G. M., (1970)
'Diffusion in Bcc Iron Base Alloys', *Metallurgical Transactions,* **1,** p. 2767-2773.

BRIGGS, J. Z. and PARKER, T. D., (1965)
'The Super 12%Cr Steels', Climax Molybdenum Company.

CAHN, J. W., (1956)
'Transformation kinetics during continuous cooling', *Acta Metallurgica,* **4,** p. 572.

CANE, B. J., (1986)
'Present Status of Predictive Methods for Remanent Life Assessment and Future Developments', *Materials Forum,* **9,** p. 5–33.

CANE, B. J. and TOWNSEND, R. D., (1984)
'Prediction of Remaining Life in Low Alloy Steels', Central Electricity Generating Board Report TPRD/L/2674/N84.

CANE, B. J. and WILLIAMS, J. A., (1987)
'Remaining Life Prediction of High Temperature Materials', *International Metals Reviews,* **32 (5),** p. 241–262.

CARINCI, G. M., HETHERINGTON, M. G. and OLSON, G. B., (1988)
'M_2C precipitation in AP1410 steel', *Journal de Physique (Paris) C6,* **49,** p. 311–316.

CARRUTHERS, R. B. and DAY, R. V., (1968)
'The Spheroidization of Some Ferritic Superheater Steels', Central Electricity Generating Board Report SSD/NE/R 138.

CARRUTHERS, R. B. and COLLINS, M. J., (1980)
Central Electricity Generating Board Report, NER/SSD/M/80/327.

CARRUTHERS, R. B. and COLLINS, M. J., (1981)
'Quantitative Microanalysis with High Spatial Resolution,' (Conf. Proc.), London, The Metals Society. p. 108–111.

CHANCE, J. and RIDLEY, N., (1981)
'Chromium Partitioning During Isothermal Transformation of a Eutectoid Steel', *Metallurgical Transactions,* **12A,** p. 1205–1213.

CHRISTIAN, J. W., (1975)
'Theory of transformations in metals and alloys', Part I, 2nd Edition, Oxford, Pergamon Press.

CHRISTIAN, J. W. and KNOWLES, K. M., (1981)
'Solid–solid phase Transformations', Eds. H.I.Aaronson et al., TMS–AIME, Warrendale, Pennsylvania. p. 1175.

CHRISTIAN, J. W. and EDMONDS, D. V., (1984)
'The Bainite Transformation', Phase Transformations in Ferrous Alloys, ASM, Metals Park, Ohio. p. 293–326.

CRANK, J., (1975)
'The mathematics of Diffusion', 2nd Edition, Oxford, Clarendon Press.

DAVISON, J. K. and YELDHAM, D. E., (1975)
'Boiler Tube Failures and their Causes', *Materials in Power Plant,* Series 3, Number 3.

DU, X., (1986)
Ph.D. Thesis, Sheffield University, England.

DUNLOP, G. L. and HONEYCOMBE, R. W. K., (1976)
'Ferrite morphologies and carbide precipitation in a Cr–Mo–V creep–resisting steel', *Metal Science,* **10,** p. 124–132.

EDMONDS, D. V. and HONEYCOMBE, R. W. K., (1973)
'Structure and properties of an isothermally transformed Fe–4Mo–0.2C alloy', *Journal of the Iron and Steel Institute,* **211,** p. 209–216.

FRANCK, F. J., TAMBUYSER, P. and ZUBANI, I., (1982)
'X–ray powder diffraction evidence for the incorporation of W and Mo into $M_{23}C_6$ extracted from high temperature alloys', *Journal of Materials Science,* **17,** p. 3057–3065.

FRIDBERG, J., TORNDAHL, L–E, and HILLERT, M., (1969)
'Diffusion in Iron', *Jernkont. Ann,* **153,** p. 263–276.

GOLDSCHMIDT, H. J., (1948)
'The Structure of Carbides in Alloy Steels', *Journal of the Iron and Steel Institute,* **160,** p. 345–362.

GOLDSTEIN, J. I., WILLIAMS, D. B. and CLIFF, G., (1986)
'Quantitative X–ray analysis' in 'Principles of Analytical Electron Microscopy', Ed. Joy *et al.* p. 155-183.

GOOCH, D. J., (1982)
'Creep Fracture of 12CrMoV steel', *Metal Science,* **16,** p. 79–88.

GOOCH, D. J., (1988)
'How much longer? – Remanent life assessment of high temperature components', in 'Central Electricity Generating Board Research', Special Issue, **21,** p. 60–67.

GREENWOOD, G. W., (1956)
'The growth of dispersed precipitates in solutions', *Acta metallurgica,* **4,** p. 243–248.

GREENWOOD, G. W., (1969)
'Particle Coarsening', in 'The mechanism of phase transformations in crystalline solids', *Institute of Metals Monograph No. 33* p. 103–110.

GULLBERG, R., (1971)
'Comparison of chromium content in $(Fe, Cr)_{23}C_6$ carbides by electron microprobe and X–ray diffraction', *Journal of the Iron and Steel Institute,* **209,** p. 71–72.

HALE, K. F., (1975)
'Creep Failure Prediction from Observation of Microstructure in 2.25Cr1Mo Steel', in 'Physical Metallurgy of Reactor Fuel Elements', The Metals Society, London. p. 193–201.

HART, R. V., (1976)
'Assessment of Remaining Creep Life Using Accelerated Stress–Rupture Tests', *Metals Technology,* **3,** p. 1–7.

HECKEL, R. W. and DE GREGORIO, R. L., (1965)
'The growth and shrinkage rates of second–phase particles of various size distributions', *Transactions of the Metallurgical Society of the A.I.M.E.,* **233,** p. 2001–2011.

HEHEMANN, R. F., (1970)
'The bainite transformation', Phase Transformations in Ferrous Alloys, ASM, Metals Park, Ohio. p. 293–326.

HILLERT, M., (1962)
'The formation of pearlite', in 'The Decomposition of austenite by diffusional processes', Eds. V. F. Zackay and H. Aaronson, Interscience, New York, NY.

HIPPSLEY, C. A., (1981)
'Precipitation sequences in the Heat–Affected–Zone of 2.25Cr1Mo steel during stress–relief heat treatment', *Metal Science,* **15,** p. 137–147.

HODSON, S. M., (1989)
MTDATA–Metallurgical and Thermochemical Databank, National Physical Laboratory, Teddington, Middlesex, U.K.

HONEYCOMBE, R. W. K., (1976)
'Transformation from Austenite in Alloy Steels', *Metallurgical Transactions A,* **7A,** p. 915–936.

HULTGREN, A., (1947)
Transactions of the American Society of Metals, **39,** p. 415.

HULTGREN, A., (1951)
Kungl. Svenska Vetenskapsakademius Handlingar, **135,** p. 403.

HYAM, E. D. and NUTTING, J., (1956)
'The tempering of plain carbon steels', *Journal of the Iron and Steel Institute,* **184,** p. 148–184.

IRVINE, K. J., CROWE, D. J. and PICKERING, F. B., (1960)
'The physical metallurgy of 12% chromium steels', *Journal of the Iron and Steel Institute,* **195,** p. 386–405.

JACK, D. H. and JACK, K. H., (1973)
'Carbides and Nitrides in Steel', *Materials Science and Engineering,* **11,** p. 1–27.

KINSMAN, K. R., EICHEN, E. and AARONSON, H. I., (1975)
'Thickening Kinetics of proeutectoid ferrite plates in Fe–C alloys', *Metallurgical Transactions A,* **6A,** p. 303–317.

KLUEH, R. L., (1978)
'Interaction solid solution hardeing in 2.25Cr1Mo steel', *Materials Science and Engineering,* **35,** p. 239–253.

KO, T. and COTTRELL, S. A., (1952)
'The formation of bainite', *Journal of the Iron and Steel Institute,* **175,** p. 307–313.

KUO, K., (1953)
'Carbides in Chromium, Molybdenum and Tungsten Steels', *Journal of the Iron and Steel Institute,* **173,** p. 363–375.

LAI, J. K. L., CHAN, S. T. and DUGGAN, B. J., (1990)
'The development of a novel temperature indicator', *High Temperature Technology,* **8,** p. 18.

LARSON, F. R. and MILLER, J., (1952)
Trans. ASME, **74,** p. 765.

LEE, Y. J., (1989)
Ph.D. Thesis, Monash University, Australia.

LEITNAKER, J. M., KLUEH, R. L., and LAING, W. R., (1975)
'The composition of eta carbide phase in $2\frac{1}{4}$Cr1Mo steel', *Metallurgical Transactions,* **6A,** p. 1949–1955.

LIFSHIFTZ, J. M. and SLYOZOV, V. V., (1961)
'The kinetics of precipitation from supersaturated solid solutions', *Journal of Physics and Chemistry of Solids,* **19,** p. 35–50.

LUNDBERG, R., WALDENSTRÖM, M. and UHRENIUS, B., (1977)
'Isothermal Sections of the Fe–Cr–C system in the Temperature Range of 873–1373K', *CALPHAD,* **1,** p. 159–199.

M^{c}LELLAN, R. B., RUDEE, M. L. and ISCHIBACHI, T., (1965)
'Thermodynamics of dilute interstitial solid solutions with dual site occupancy and its applications to the diffusion of carbon in α–iron', *Trans. Met. Soc. A.I.M.E.,* **233,** p.1938–1948.

MIDDLETON, C. J., (1986)
Central Electricity Generating Board Report TPRD/L/MT0380/M86.

MILLER, M. K. and SMITH, G. D. W., (1989)
'Atom probe microanalysis; Principles and applications to materials problems', Materials Research Society.

MUKHERJEE, T., STUMPF, W. E., and SELLARS, C. M., (1968)
'Quantitative assessment of extraction replicas for particle analysis', *Journal of Materials Science,* **3,** p. 127–135.

MUKHERJEE, T., STUMPF, W. E., SELLARS, C. M. and TEGART, W. J. MCG., (1969)
'Kinetics of coarsening of carbides in chromium steels at 700°C ', *Journal of the Iron and Steel Institute,* p. 621–631

OHMORI, Y. and HONEYCOMBE, R. W. K., (1971)
'The isothermal transformation of plain carbon steels', Proceedings ICSTIS *Supplementary transactions of the Iron and Steel Institute of Japan,* **11,** p. 1160–1164.

OKA, M. and OKAMOTO, H., (1986)
'Isothermal transformations in hypereutectoid steels', in Proceedings of International Conference on martensitic transformations, ICOMAT '86, Japan Institute of Metals, p. 271–275.

OLSON, G. B., KINKUS, T. J. and MONTGOMERY, J. S., (1991)
'APFIM study of multicomponent M_2C carbide precipitation in AF1410 steel', *Surface Science,* **246,** p. 238–245.

ORIANI, R. A., (1964)
'Ostwald ripening of precipitates in solid matrices', *Acta Metallurgica,* **12,** p. 1399–1409.

PILLING, J. and RIDLEY, N., (1982)
'Tempering of 2.25 Pct Cr–1 Pct Mo Low Carbon Steels', *Metallurgical Transactions,* **13A,** p. 557–563.

PITSCH, W. and SCHRADER, A., (1958)
Arch. Eisenhuettenw., **29,** p. 715

PULS, M. P. and KIRKALDY, J. S., (1972)
'The Pearlite Reaction', *Metallurgical Transactions A,* **3A,** p.2777–2796.

ROBINSON, E. L., (1938)
Trans. ASME, **60,** p. 253.

SELLARS, C. M., (1974)
'Creep Strength in Steel and High Temperature Alloys', The Metals Society, London. p. 20–30.

SHA, W., CHANG, L., SMITH, G. D. W., LUI CHENG and MITTEMEIJER, E. J., (1992)
'Some aspects of atom probe analysis of Fe–C and Fe–N systems', *Surface Science,* **266,** p. 416–423.

SHAMMAS, M. S., (1987)
'Remanent Life Assessment of the Ferritic Weld Heat Affected Zones by a Metallographic Measurement of Cavitation Damage–The 'A' Parameter', Central Electricity Generating Board Report, TPRD/L/3200/R87.

SHAW, S. W. K. and QUARRELL, A. G., (1957)
'The Formation of Carbides in Low–Carbon Chromium–Vanadium Steels at 700°C ', *Journal of the Iron and Steel Institute,* **185,** p. 10–22.

SMITH, R. and NUTTING, J., (1957)
British Journal of Applied Physics, **7,** p. 214–217.

SMITH, R. and NUTTING, J., (1957)
'The Tempering of Low–Alloy Creep–Resistant Steels containing Chromium, Molybdenum, and Vanadium', *Journal of the Iron and Steel Institute,* **187,** p. 314–329.

STARK, I., SMITH, G. D. W., and BHADESHIA, H. K. D. B., (1987)
'The element redistribution associated with the Incomplete–Reaction Phenomenon in Bainitic Steels: An atom probe investigation', Proceedings of an International Conference, 'Phase transformations 1987', Institute of Metals, London, Edited by G.W. Lorimer. p. 211–215.

STEVENS, R. A. and LONSDALE, D., (1987)
'Electrolytic Extraction of Carbide Precipitates from Low Alloy Ferritic Steel Power Plant Components', Central Electricity Generating Board Report OED/STB(S)/87/0028/R.

STRANGWOOD, M. and BHADESHIA, H. K. D. H., (1987)
'Solute segregation, oxygen content, and the transformation start temperature of steel welds', Proceedings of International Conference on Welding Metallurgy of Structural Steels, AIME, Warrendale, Pennslyvania, Edited by J.Y. Koo p. 495–504.

STUART, H. and RIDLEY, N., (1966)
'Thermal Expansion of Cementite and Other Phases', *Journal of the Iron and Steel Institute,* **204,** p. 711–717.

TILLMAN, C. J. and EDMONDS, D. V., (1974)
'Alloy carbide precipitation and aging during high–temperature isothermal decomposition of an Fe–4Mo–0.2C alloy steel', *Metals Technology,* **1,** p. 456–461.

TITCHMARSH, J. M., (1978)
'The Identification of Second–Phase Particles in Steels using an Analytical Transmission Electron Microscope', in Proc. 9th Inst. Congress on Electron Microscopy, J.M. Sturgess, ed., Microscopical Society of Canada, Toronto. **1** p. 618–619.

TOFT, L. H. and MARSDEN, R. A., (1961)
'The Structure and Properties of 1Cr0.5Mo Steel After Service in Central Electricity Generating Board Power Stations', *Journal of the Iron and Steel Institute, Special Report 70,* p. 276–294.

VENGOPULAN, D. and KIRKALDY, J. S., (1978)
'Hardenability Concepts with Applications to Steels', Conference Proceedings, 249, New York, AIME.

WADA, M., HOSOI, K. and NISHIKAWA, O., (1982)
'FIM observation of 2.25Cr1Mo steel', *Acta Metallurgica,* **30,** p. 1013–1018.

WAGNER, C., (1961)
'Theorie der Alterung von Niederschlägen durch Umlösen', *Z. Elektrochem,* **65,** p. 581–591.

WAUGH, A. R., RICHARDSON, C. H. and JENKINS, R., (1992)
'APFIM 200 – A reflectron–based atom probe', *Surface Science,* **266,** p. 501–505.

WESTGREN, A., PHRAGMÉN G. and NEGRESCO, T. R., (1928)
'On the structure of the iron–chromium–carbon system', *Journal of the Iron and Steel Institute,* **117(1),** p. 383–400.

WILLIAMS, P. R., MILLER, M. K., BEAVEN, P. A. and SMITH, G. D. W., (1979)
'Fine scale analysis of partitioning in pearlitic steels,' in Proceedings of the York phase transformations meeting, **2,** p. 11–98.

WILSON, M., (1986)
'The Assessment of the Remaining Creep Life of Carbon and Low Alloy Steel Power Plant Components', *Materials Forum,* **9,** p. 53–66.

WOODFORD, D. A., (1974)
Proc. International conference on Creep and Fatigue in Elevated Temperature Applications, Philadelphia, 1973. Sheffield 1974.

WOODHEAD, J. H. and QUARRELL, A. G., (1965)
'Role of Carbides in Low–alloy creep Resisting Steels', *Journal of the Iron and Steel Institute,* **203,** p. 605–620.

YAKEL, H. L., (1985)
'Crystal structures of stable and metastable iron–containing carbides', *International Metals Reviews,* **30(1),** p. 17–40.

YU, J., (1989)
'Carbide stability diagrams in 2.25Cr1Mo steels', *Metallurgical Transactions A,* **20A,** p. 1561–1564.